Recent Research Topics of Solid State Electronics Laboratory in the Department of Physics in Tsing Hua University

Juh Tzeng Lue

What includes in solid state electronic laboratory?

The characterization of amorphous carbon nitride films grown by RFCVD method

CN structure

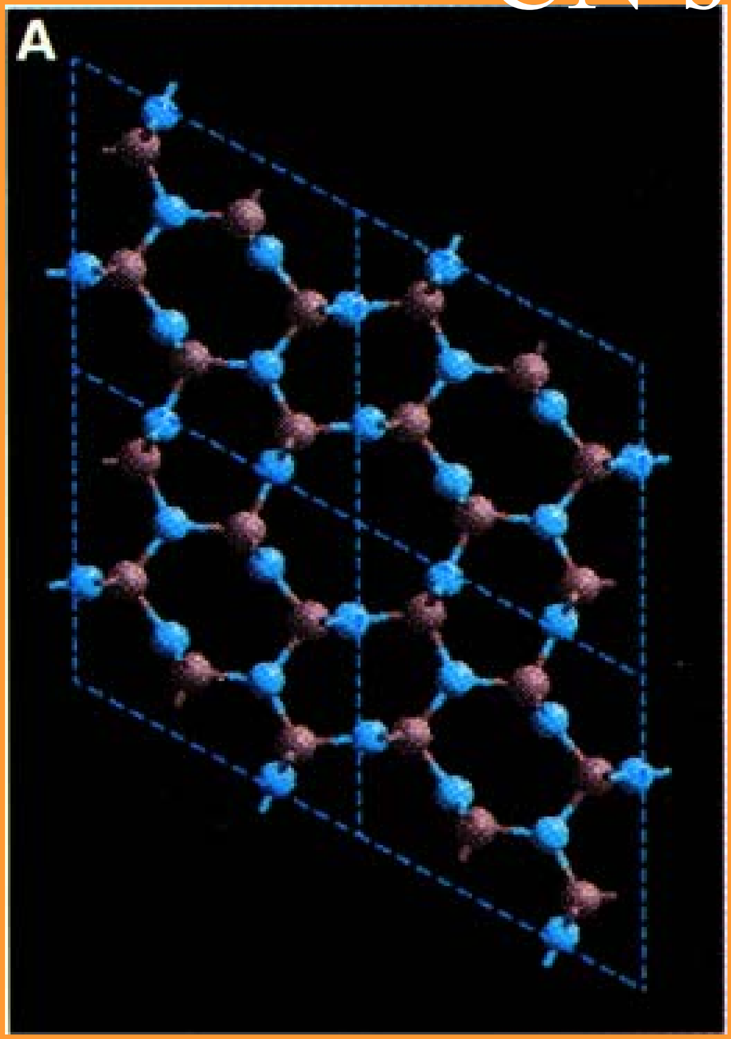

•Introduction

In 1985, Cohen developed an empirical model to express the bulk modulus of covalent solid.

Liu and Cohen predicted that the bulk modulus of hypothetical compound β -C3N4 may be close to that of diamond which has a structure similar to the β -Si3N4.

In addition to super hardness, it exhibits to good insulating property.

Representation of the β -C3N4. The carbon and nitrogen atoms are depicted as gray and blue spheres, respectively.

Structure of carbon nonatubes

Carbon: $1s^2$, $2s^1$ $2p^3$

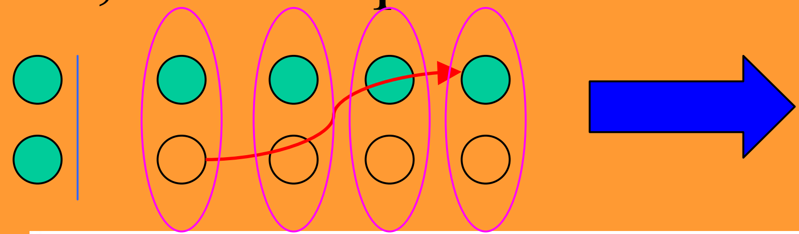

sp^1, sp^2, sp^3

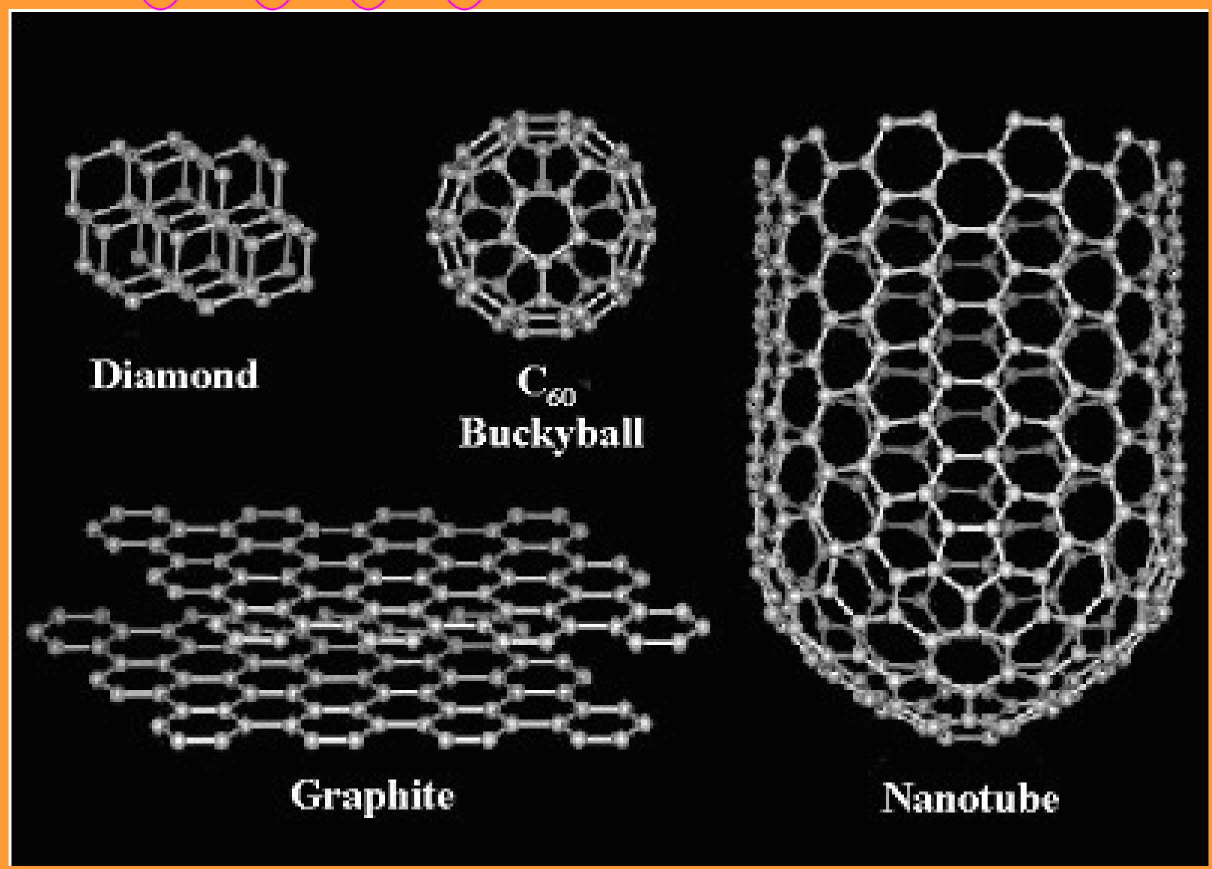

Sumio Iijma

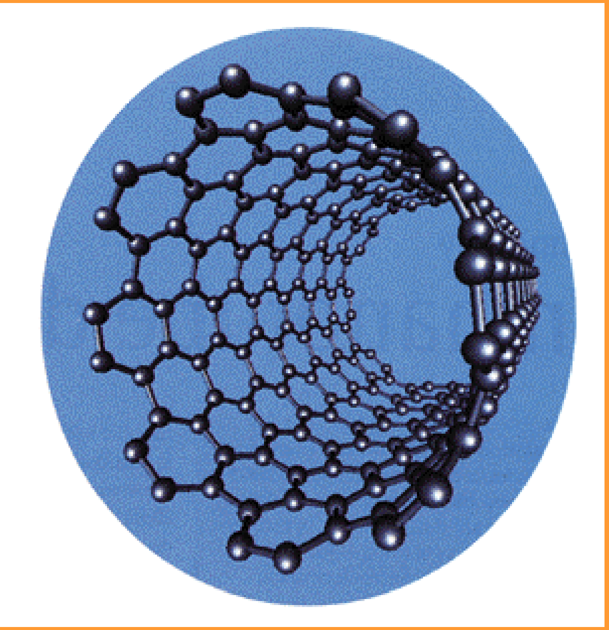

Single-walled carbon nanotube, SWCNT

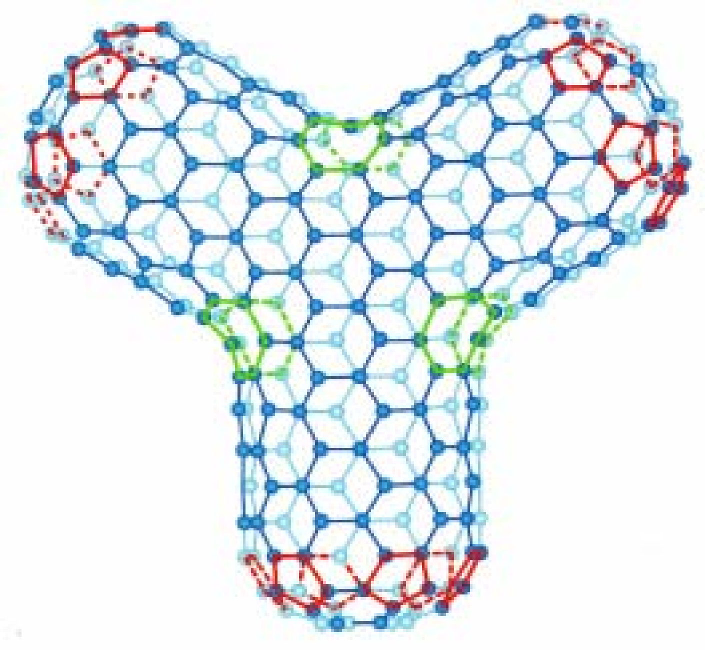

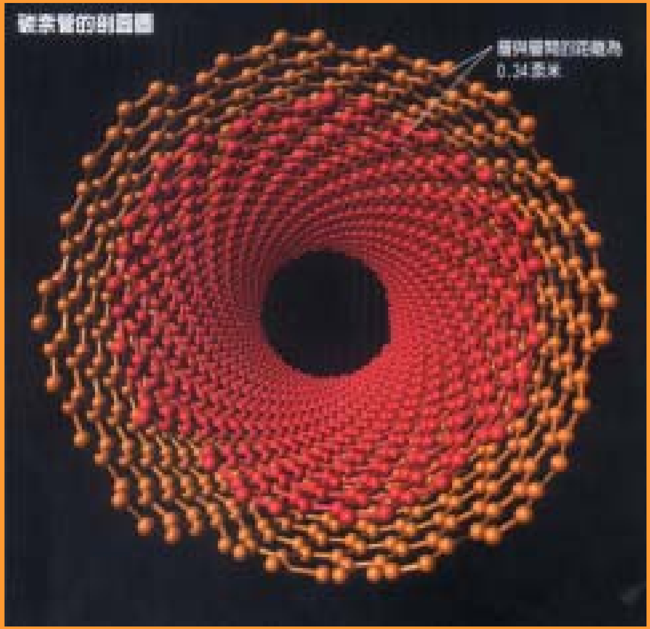

Multi-walled carbon nanotube, MWCNT

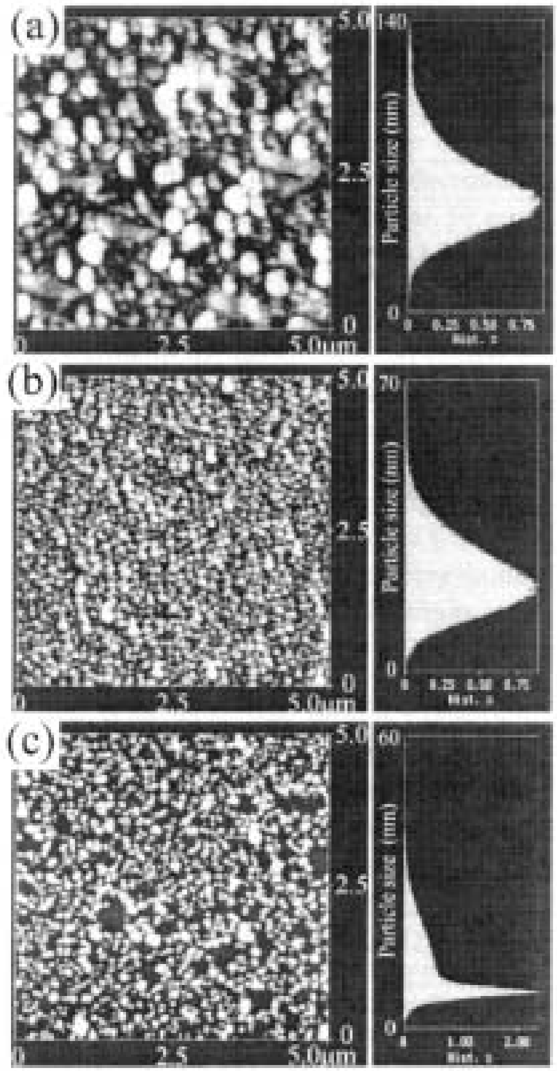

FIG. 2. AFM images of a Fe film annealed at 660 °C for 10 min. The corresponding thickness of the Fe film is 20, 10, and 5 nm in images (a), (b), and (c), respectively. The particle size distribution was derived from the AFM images.

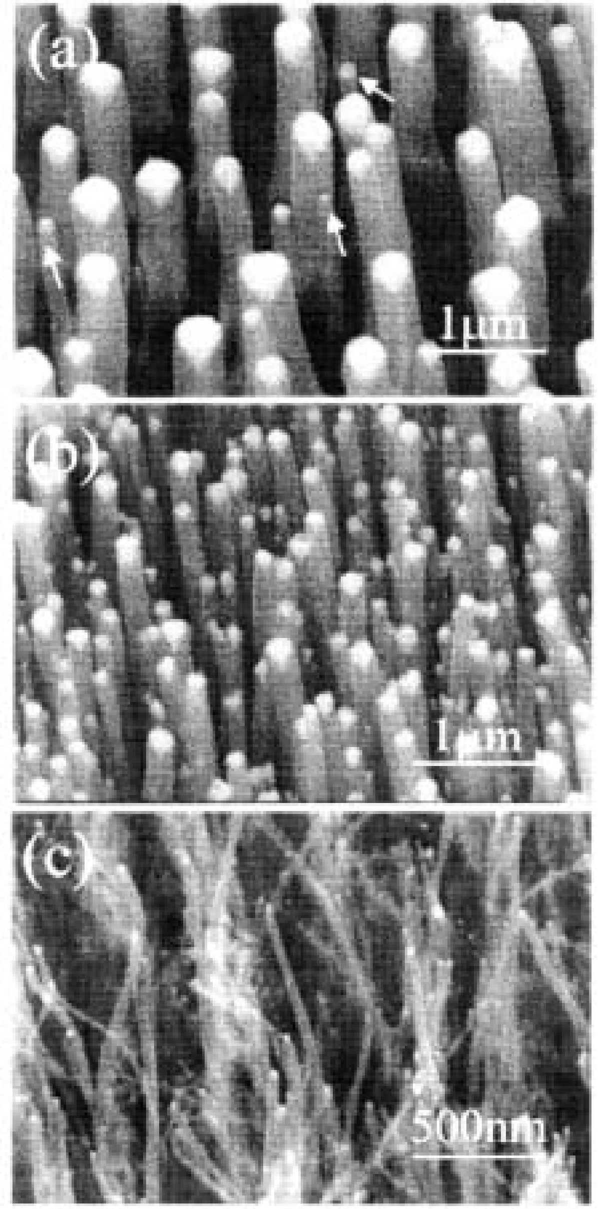

自製的微波/射頻輔助熱燈絲化學氣相沉積法製作

根部成長

單層奈米管(SWNT)的影像

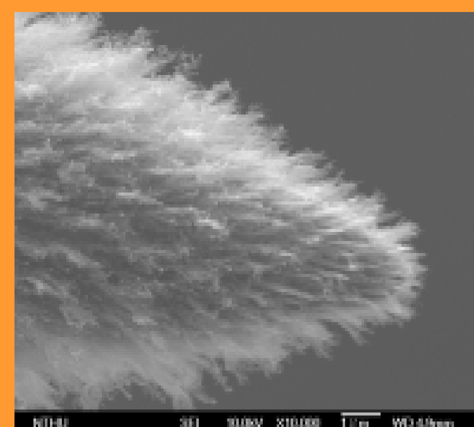

頂端成長

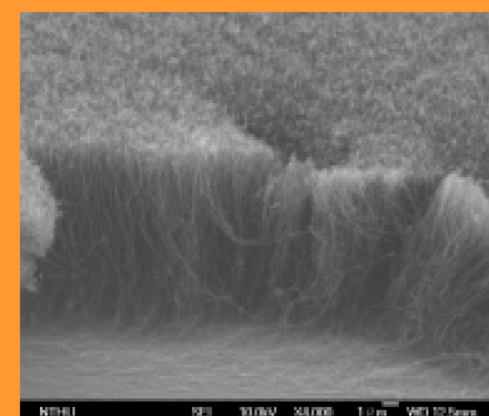

大面積,高密度均勻分散的指向性多層奈米管(MWNT)

變溫場發射結果

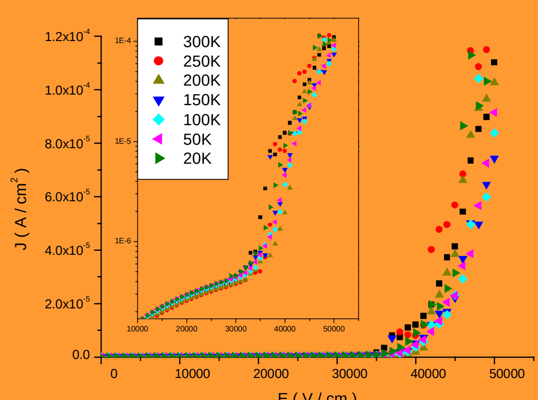

溫度變化由室溫到低溫
(300K ~20K)
結果顯示場發射特性並不隨溫度降低而改變


NTHU
SEI
10.0kV
X33,000
100nm
WD 9.0mm

The model dwelled in reference (C.L. Chen, C.S. Chen, J.T. Lue, Solid State Electronics 44 (2000) 1733.

$$J_{total} = J_c + J_v$$

$$J_{total} = a_1 T^2 e^{-\theta/kT} e^{\frac{-b\chi^{3/2}}{\beta F}} + a_2 \frac{(\beta F)^2}{\chi + E_g} e^{\frac{-b(\chi+E_g)^{3/2}}{\beta F}}$$

$$a_1 = \frac{qmk^2}{2\pi^2\hbar^3} \quad , \qquad a_2 = \frac{q^3}{16\pi^2\hbar\ t(y)} \quad ,$$

$$b = \frac{4\sqrt{2m}}{3q\hbar} v(y) \quad ,$$

Where ***F*** is the external electrical field, β is the field enhancement factor, ***v(y)*** and ***t(y)*** are tabulated functions involving elliptic integrals, ***x*** is the electron affinity, $\theta = E_{cs} - E_f$ is the difference energy between interface conduction band and Fermal level.

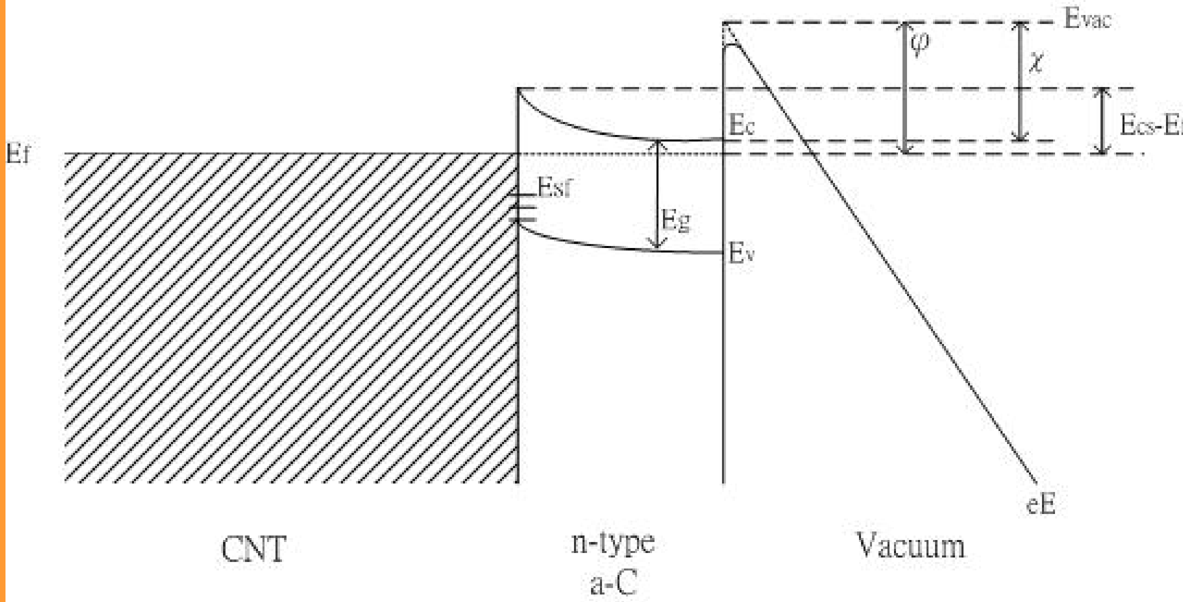
Evac
φ
χ
Ecs-Ef
Ec
Ef
Esf
Eg
Ev
eE
CNT
n-type
a-C
Vacuum

High T

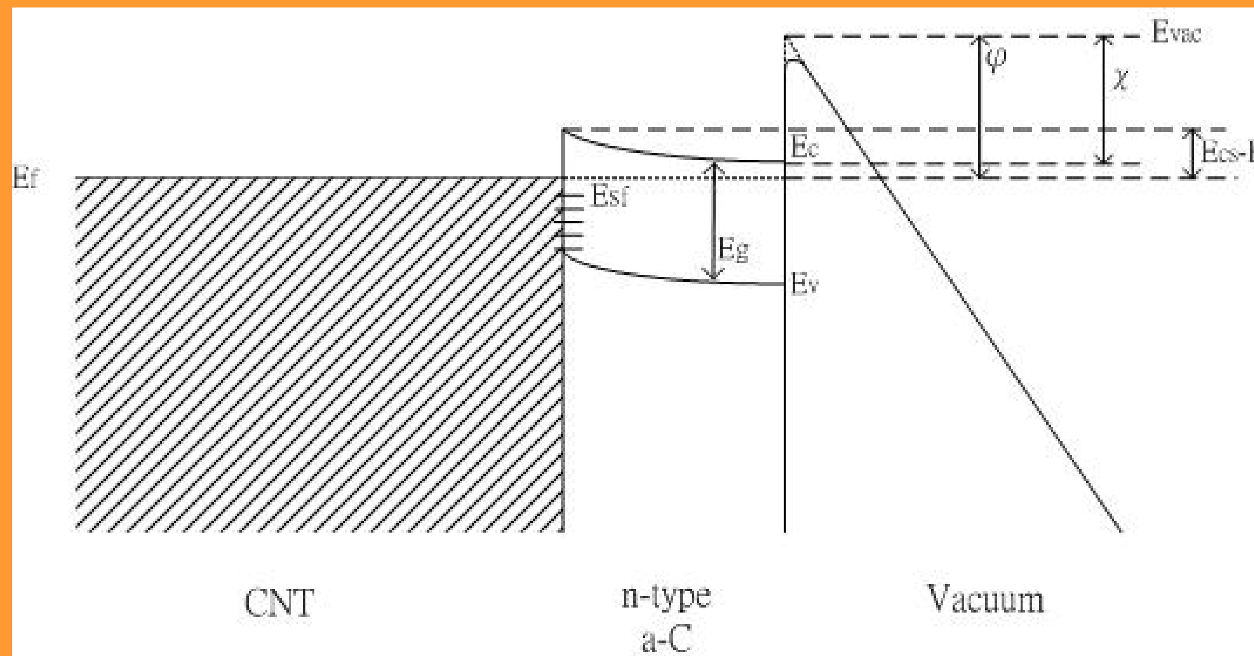
Evac
φ
χ
Ecs-Ef
Ec
Ef
Esf
Eg
Ev
CNT
n-type
a-C
Vacuum

Low T

國立清華大學物理系　　呂助增教授

微波頻段下正常態與非正常態金屬膜之電導率與頻率及溫度之關係

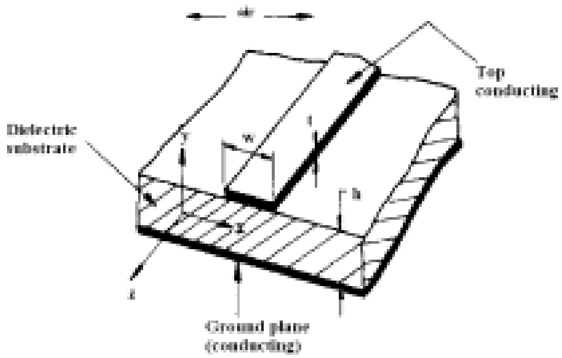

自行設計微帶傳輸線結構圖

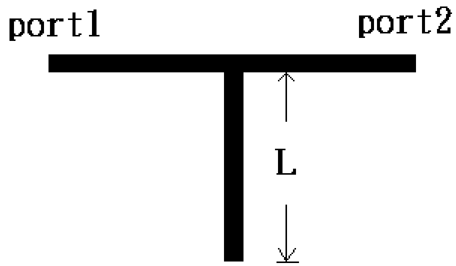

T型共振腔結構

實驗結果

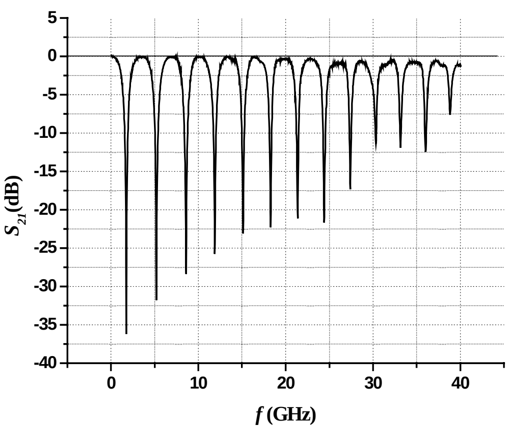

頻率響應

在強侷限效應下,電子傳播會因電磁波頻率驅動聲子而輔助,所以電導率和頻率成正比.

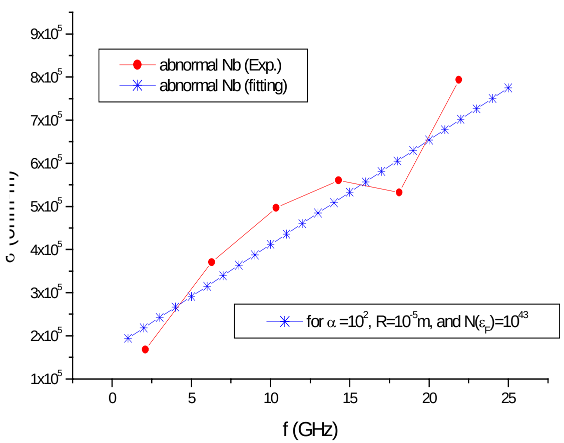

鈮金屬薄膜結果

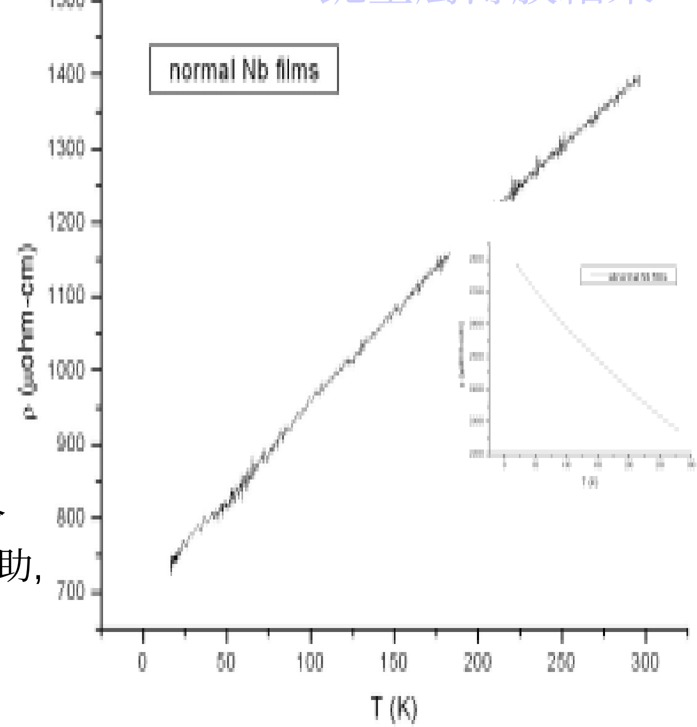

大圖為一般成長條件下成長的鈮金屬膜,表面較平滑導電性較佳,當溫度升高時,電子受到較多的雜質散射,所以電阻率升高;而小圖則為特別成長條件下成長的鈮金屬膜,表面有島狀分佈,所以電性較差,然而當溫度上升時,電子卻能因熱聲子的輔助而跳過島嶼,反而電阻率下降.

Conductivity dependence on f

$$\sigma(f) = 5.12 \times 10^{-38} \times R^2 N e^{-2\alpha R - \frac{5.8\times 10^{19}}{R^3 N}} f$$

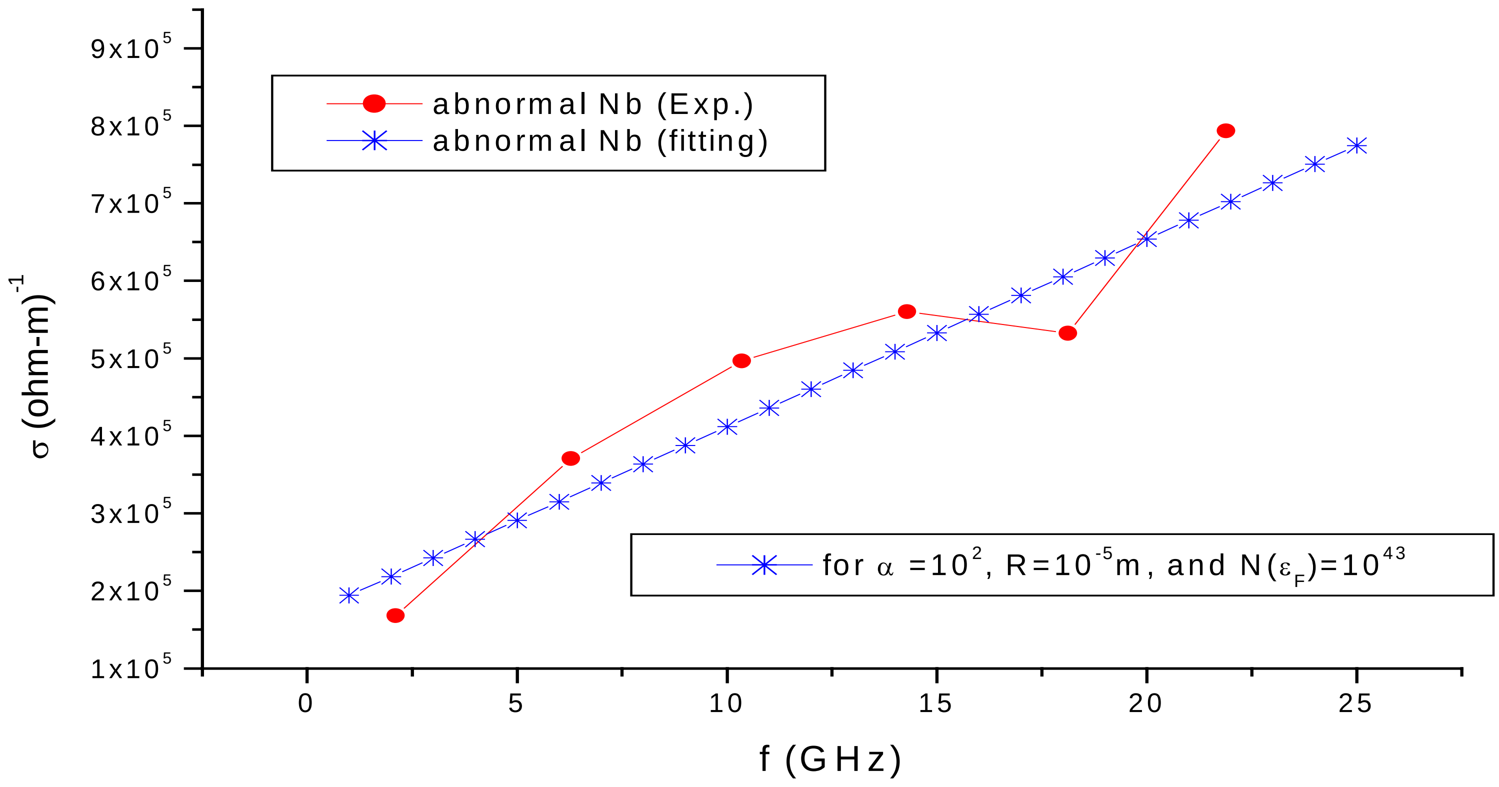

Table 1. The measured data for various Q factors to derive the dielectric constant of silver nanoparticles where f_0 (GHz) is the resonance frequency, Q_0 is the empty Q factor, Q_{01} is that for pure alumina powder and Q_{02} is that for filled with mixed powder with a filling factor $f = 100$.

Particle size (Å)	f_0 (GHz)	Q_0	Q_{01}	Q_{02}	ε
310	14.164 125 000	3061	2288	1462	−44.06 + 7.89i
371	14.166 687 500	3061	2288	1688	−47.12 + 5.32i

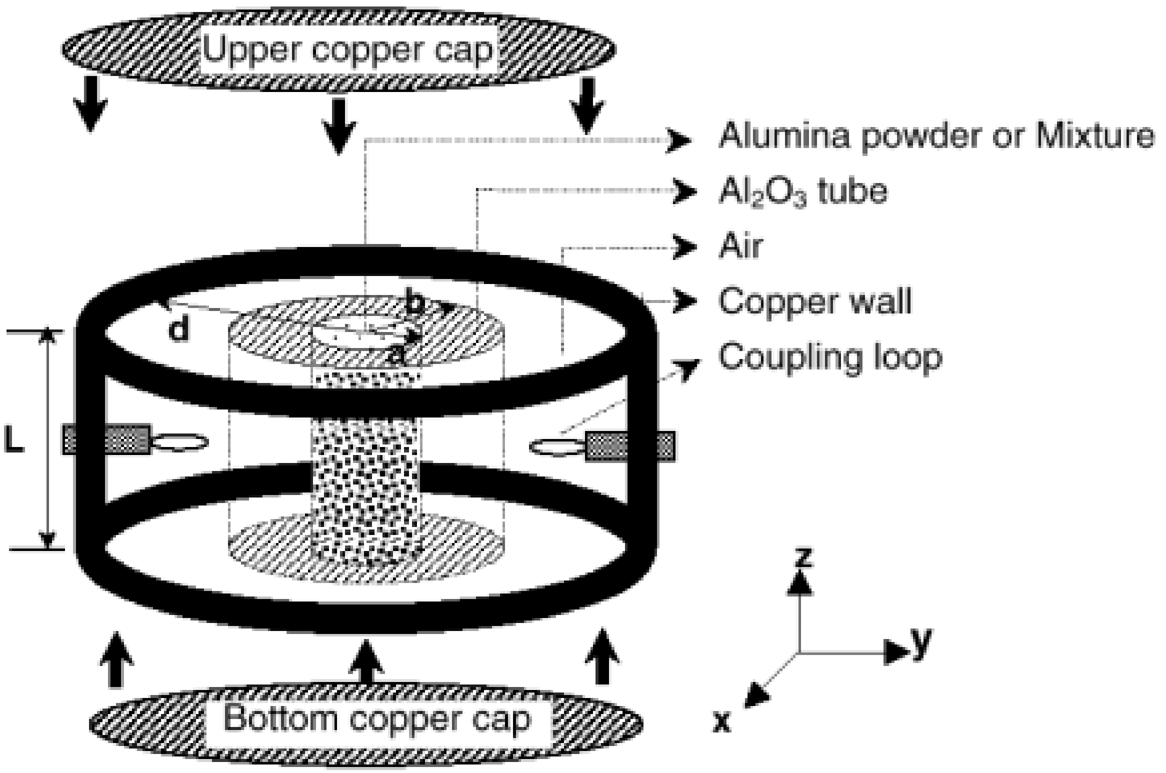

Figure 1. Construction detail of the dielectric resonator in which the radii of the inner hole, the sapphire ring and copper cavity are a, b and d, respectively, with a length of L.

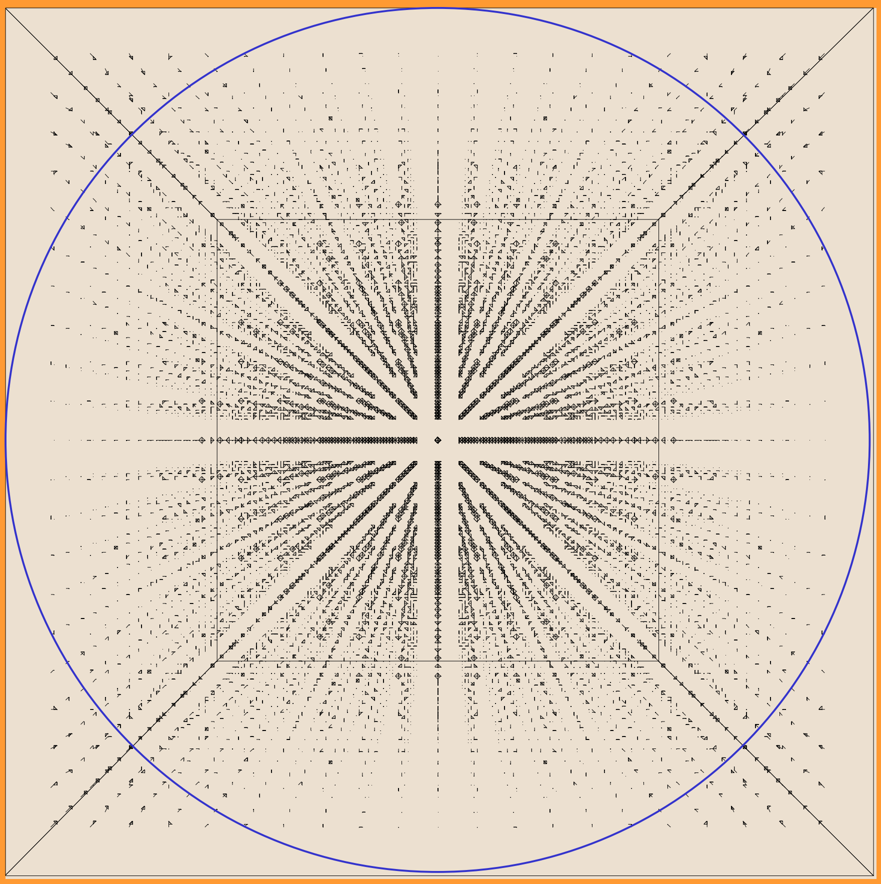

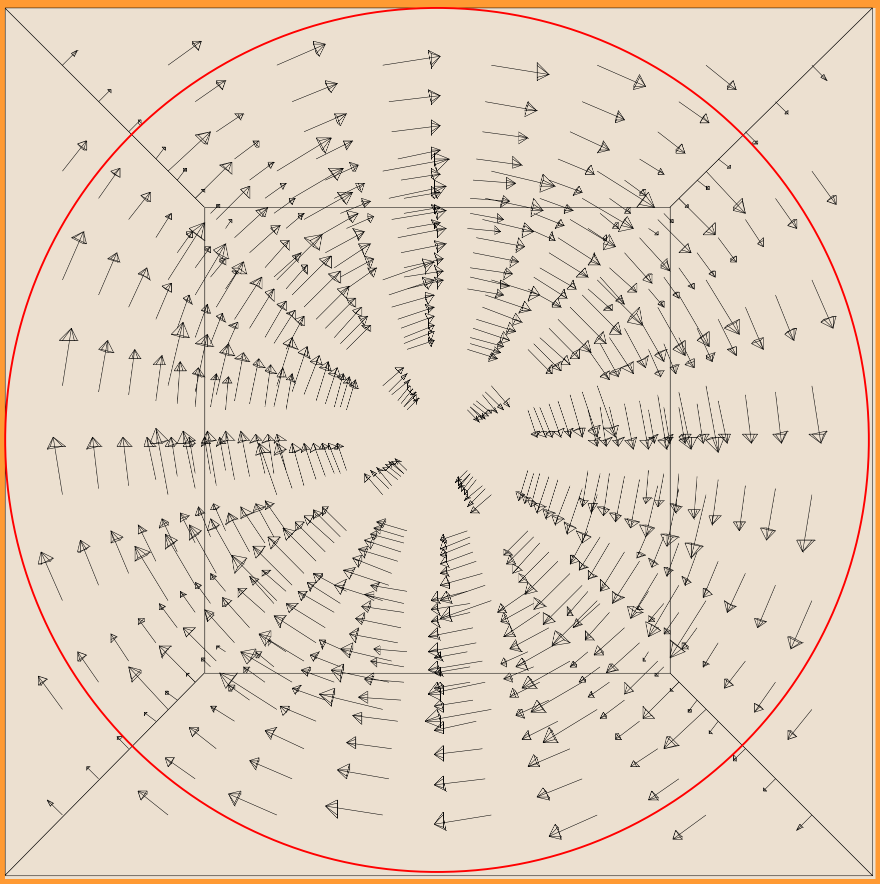

電場　　　　磁場

Microwave DR for penetration depth

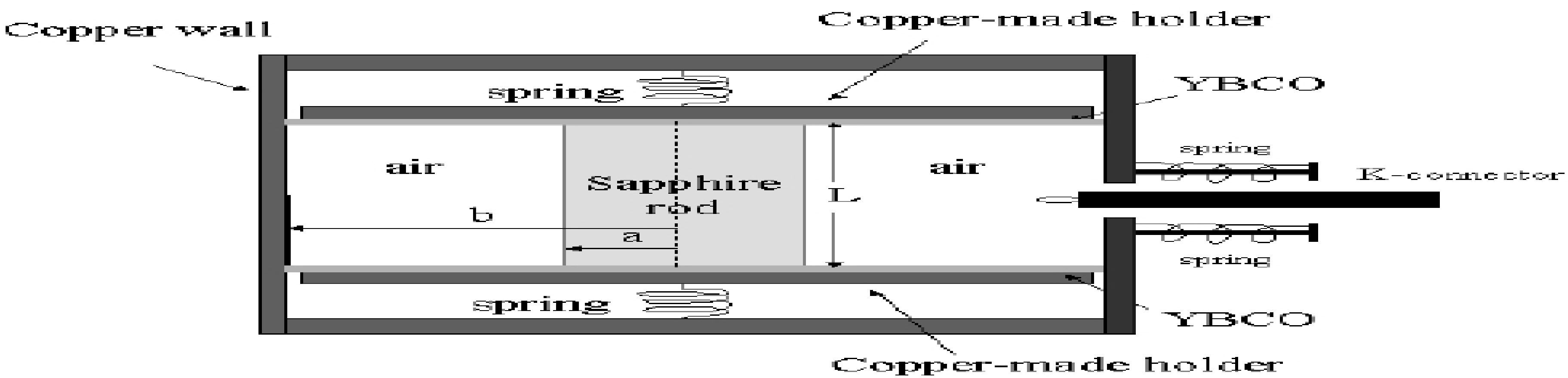

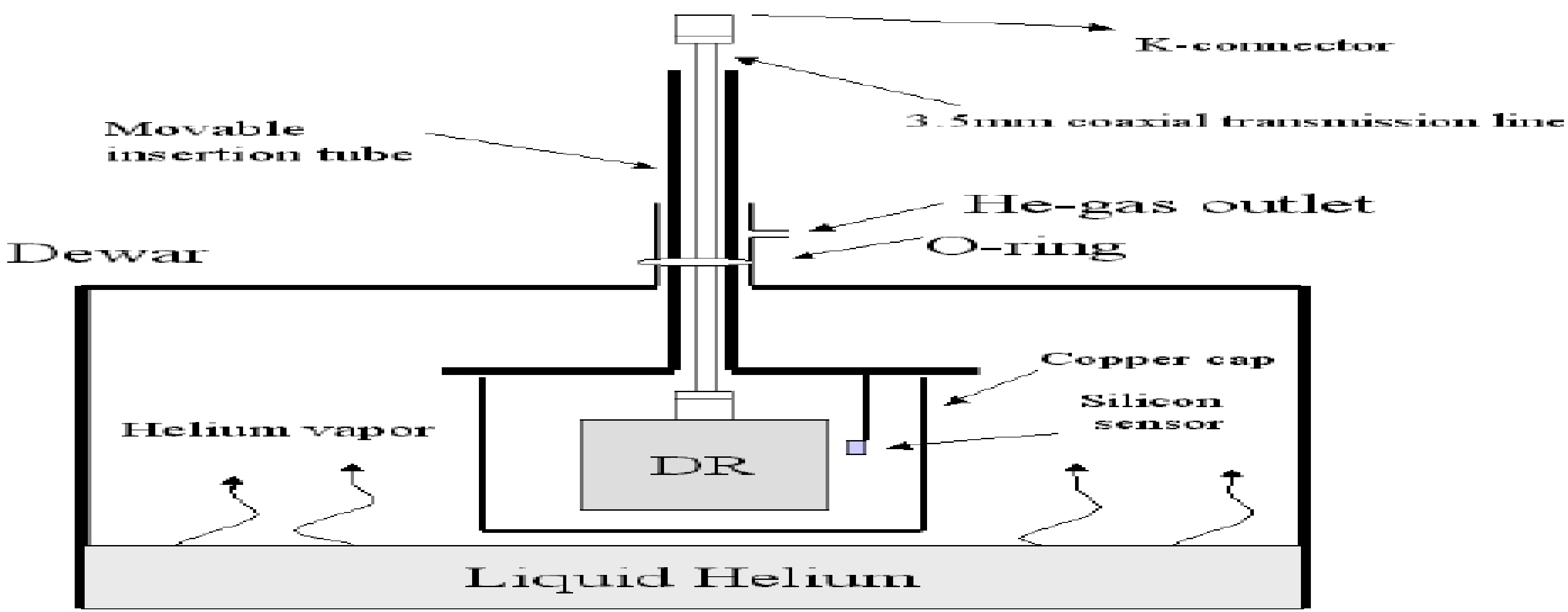

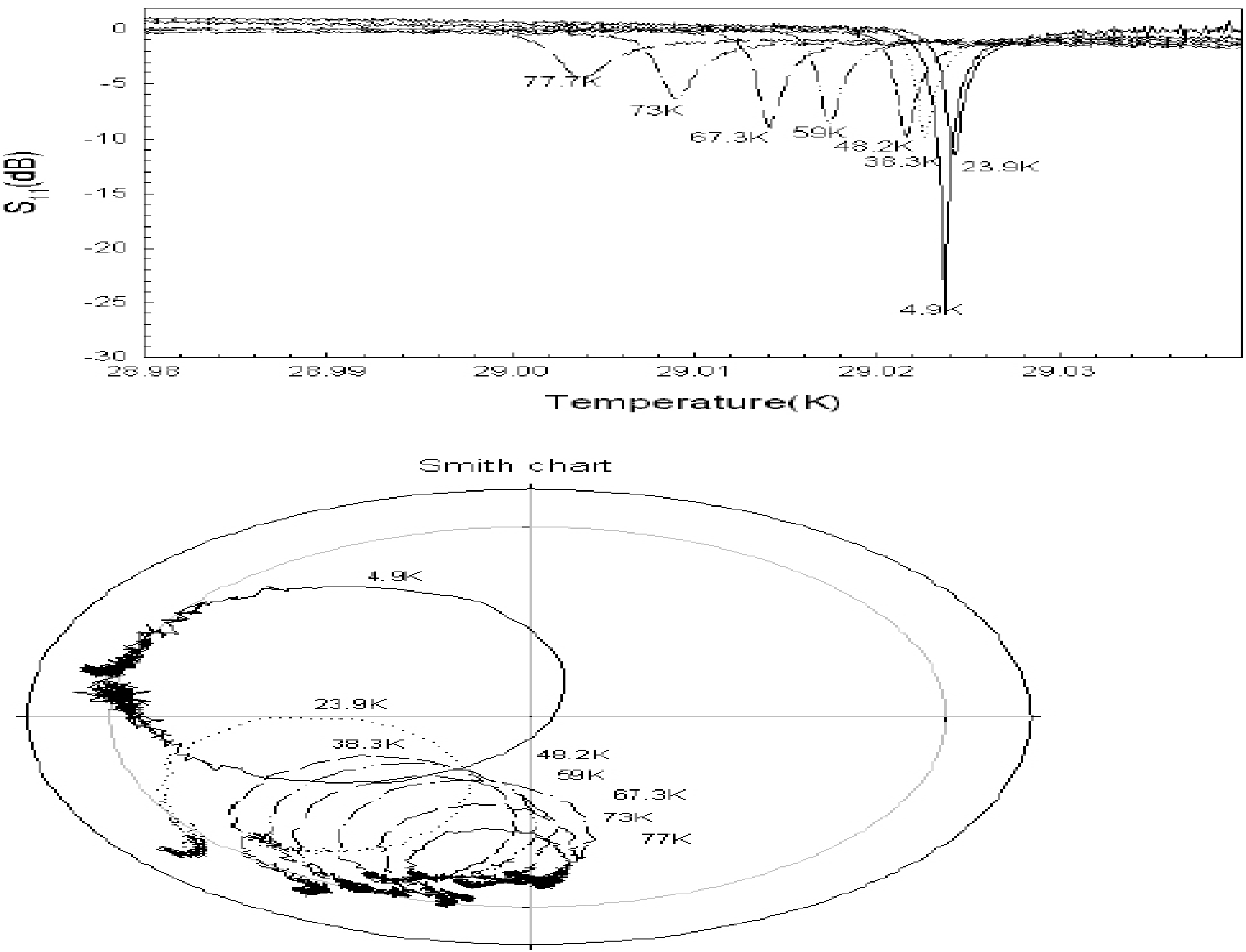

0
-5
-10
-15
-20
-25
-30
S_{11}(dB)
28.98
28.99
29.00
29.01
29.02
29.03
Temperature(K)
77.7K
73K
67.3K
59K
48.2K
38.3K
23.9K
4.9K
Smith chart
4.9K
23.9K
38.3K
48.2K
59K
67.3K
73K
77K

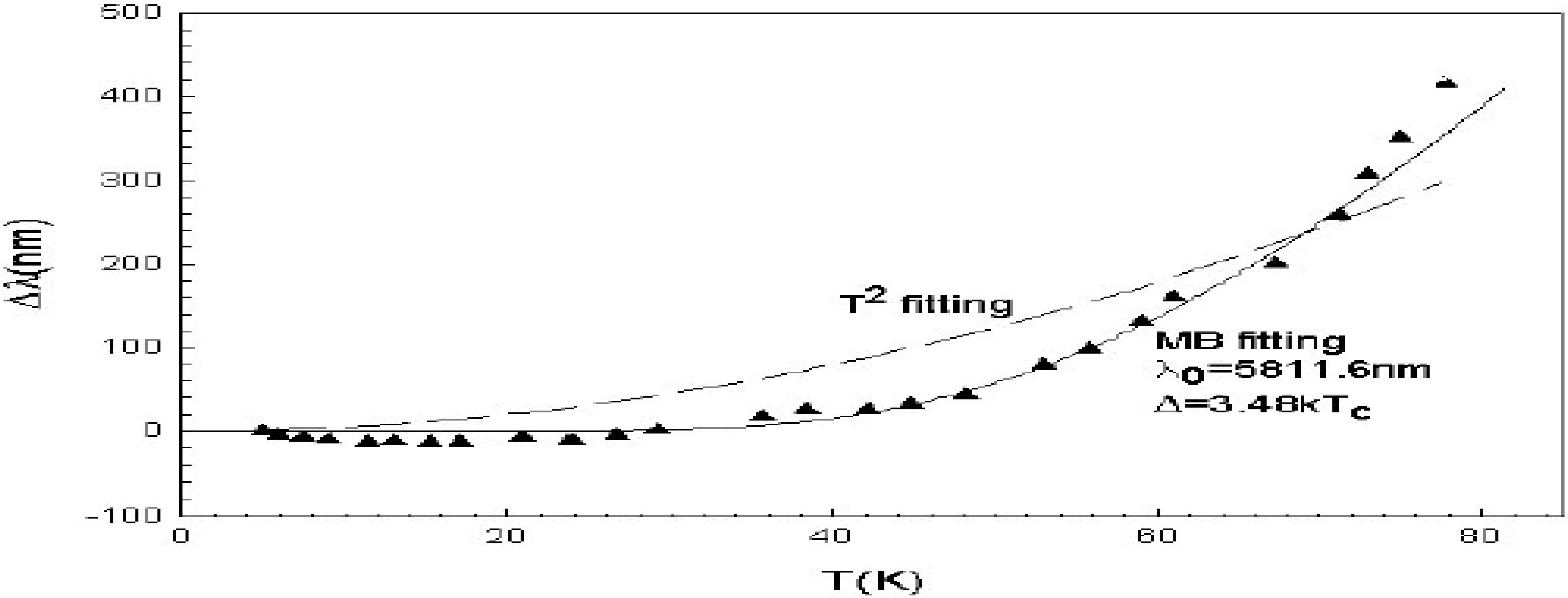

T² fitting
MB fitting
λ0=5811.6nm
Δ=3.48kTc
Δλ(nm)
T(K)

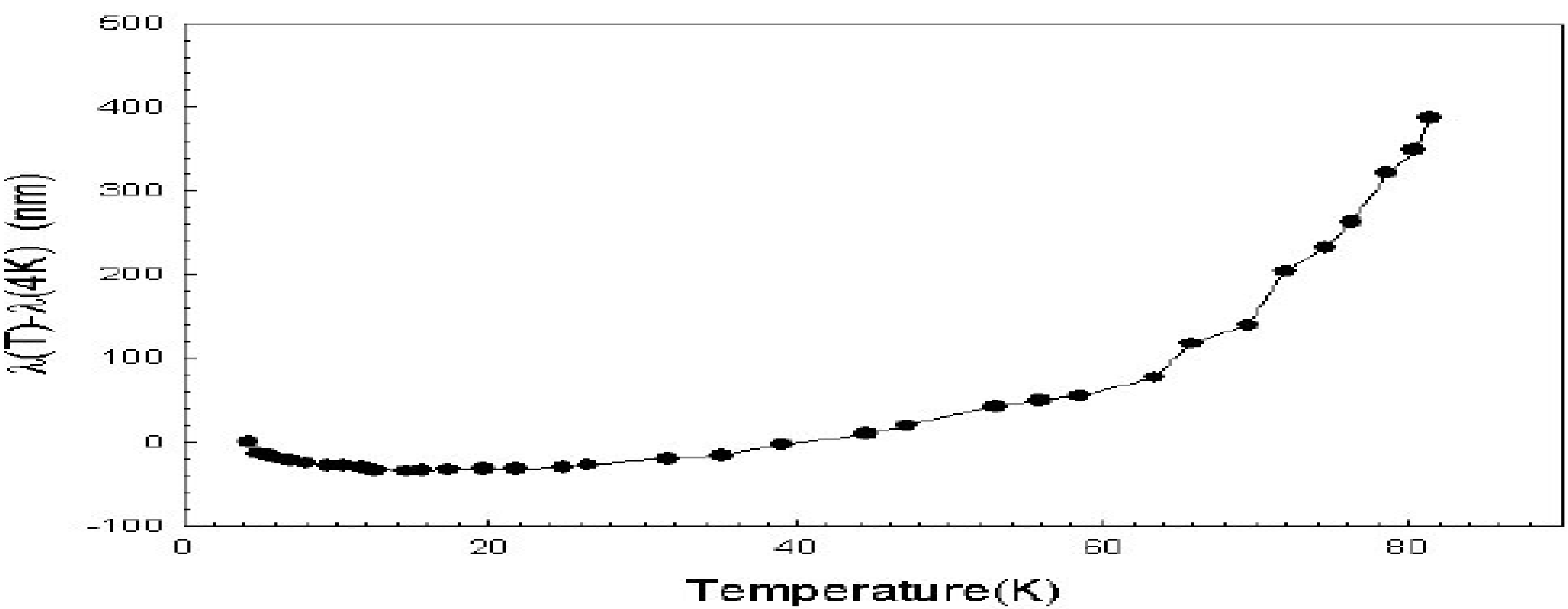

λ(T)-λ(4K) (nm)
Temperature(K)

Narrow band rejection filter composed of metal/insulator multilayers

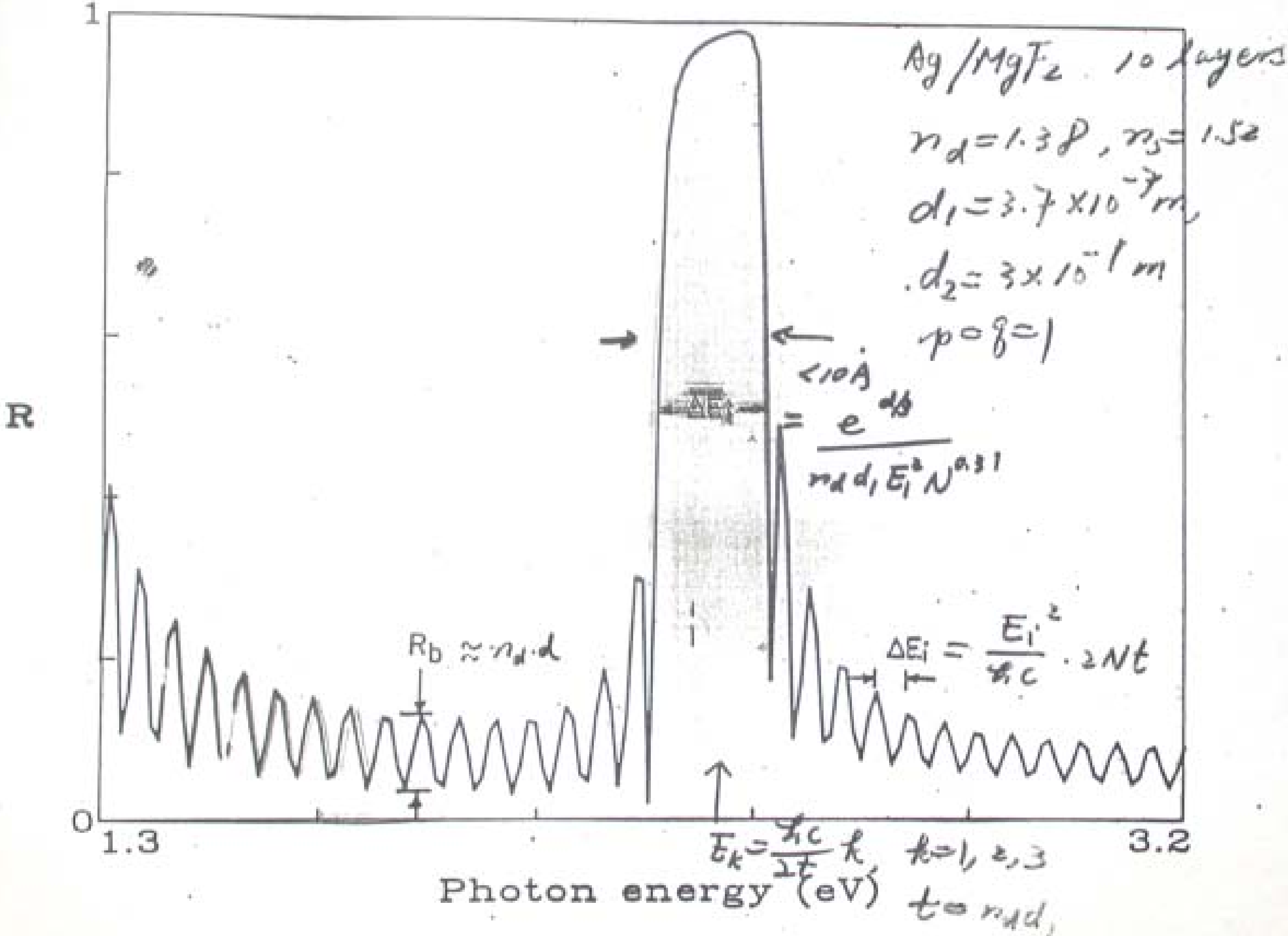

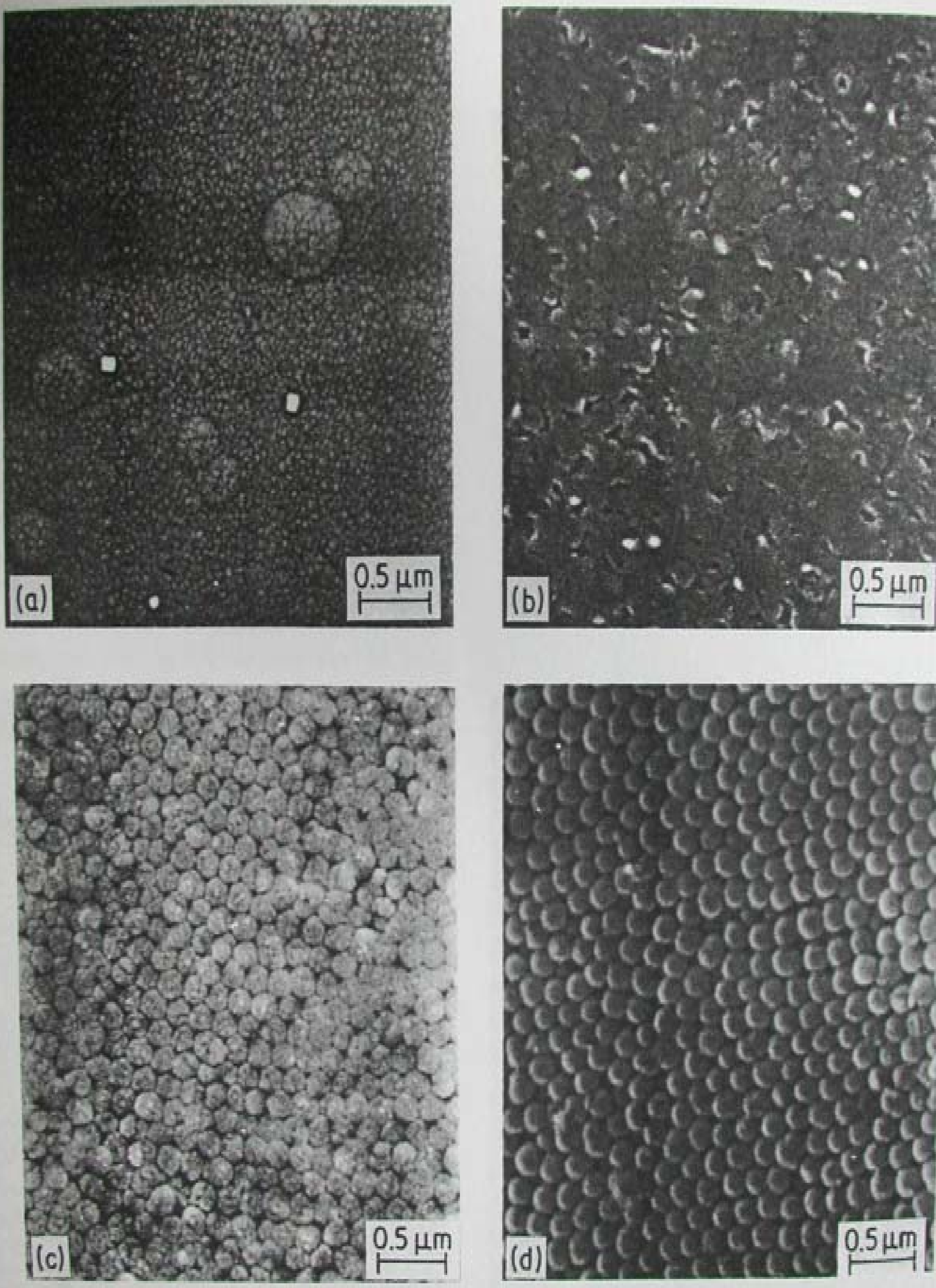
(a)
0.5 µm
(b)
0.5 µm
(c)
0.5 µm
(d)
0.5 µm

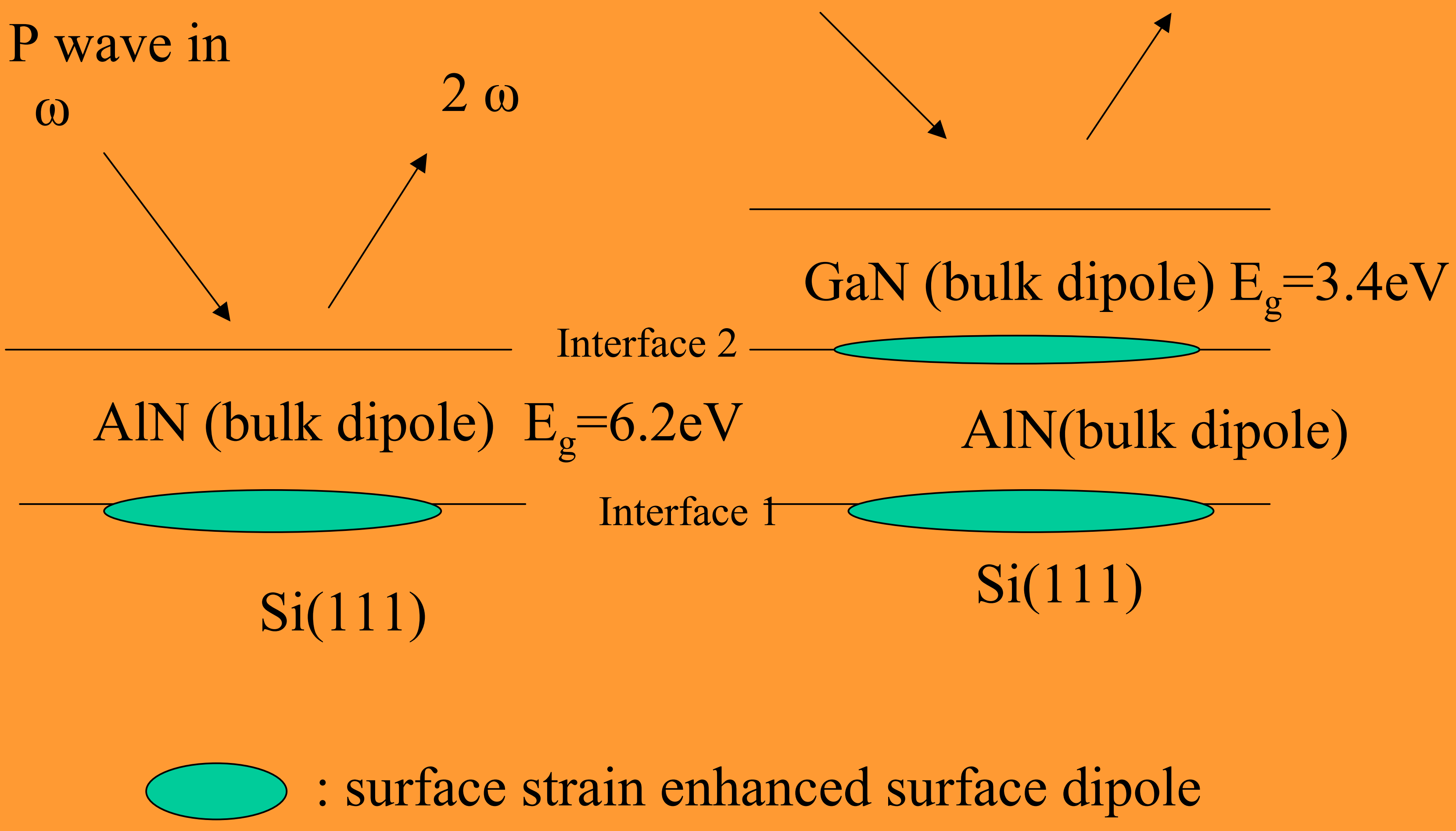

P wave in ω
2 ω
GaN (bulk dipole) E$_g$=3.4eV
Interface 2
AlN (bulk dipole) E$_g$=6.2eV
AlN(bulk dipole)
Interface 1
Si(111)
Si(111)
: surface strain enhanced surface dipole

For either s- or p-polarized pump radiation, the SH field of Si(111) can be expressed as

$$E_p^{2\omega} = a_p(\theta) + c_p \cos(3\varphi)$$

$$E_s^{2\omega} = b_s \sin(3\varphi)$$

If $a_p / c_p = 0$, the SH pattern is sixfold symmetry;
if $a_p / c_p = 1$, it is threefold.

a_p: isotropic constant

b_s, c_p: anisotropic constants

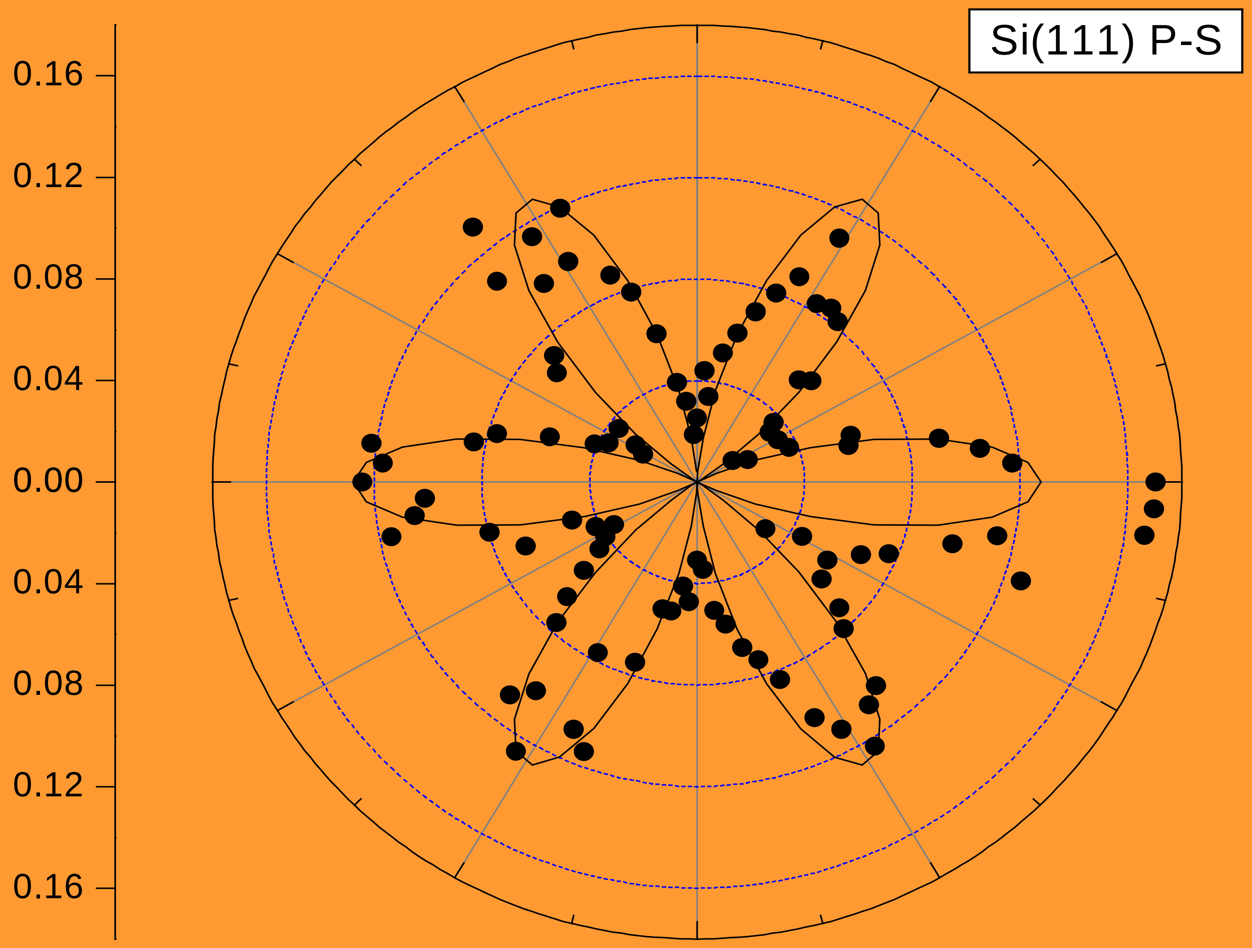

Si(111) P-S
0.16
0.12
0.08
0.04
0.00
0.04
0.08
0.12
0.16

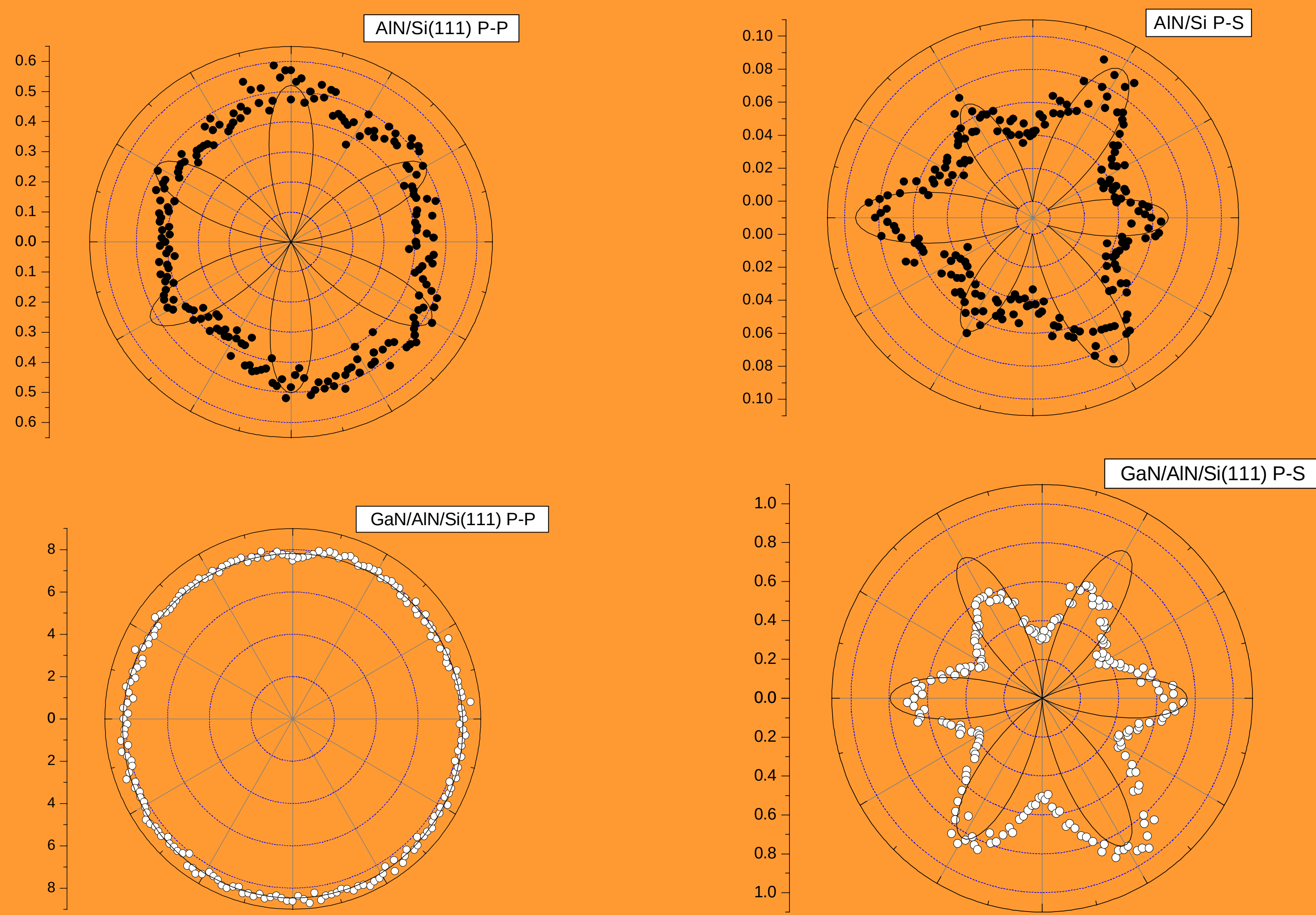
AlN/Si(111) P-P
AlN/Si P-S
GaN/AlN/Si(111) P-P
GaN/AlN/Si(111) P-S
0.6
0.5
0.4
0.3
0.2
0.1
0.0
0.10
0.08
0.06
0.04
0.02
0.00
8
6
4
2
0
1.0
0.8

Proposed model

$$H = \sum_{i,j}^{N} J_{ij}\sigma_i^z\sigma_j^z - g\sum_i^N (\sigma_i^x \cdot n^x)^2 \quad \ldots\ldots\ldots\ldots\ldots(1)$$

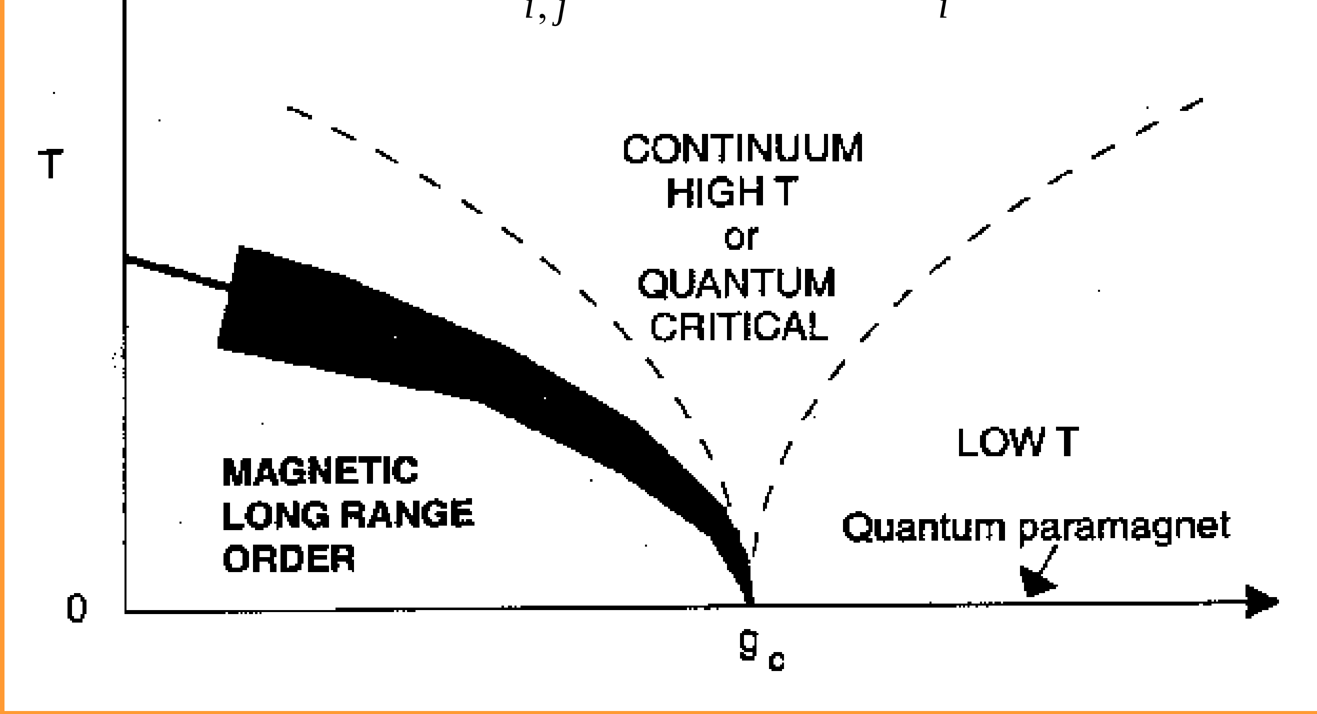

g is the anisotropy energy density

Single domain particles

. Nanoparticles usually exhibit an uniaxial magnetic anisotropy

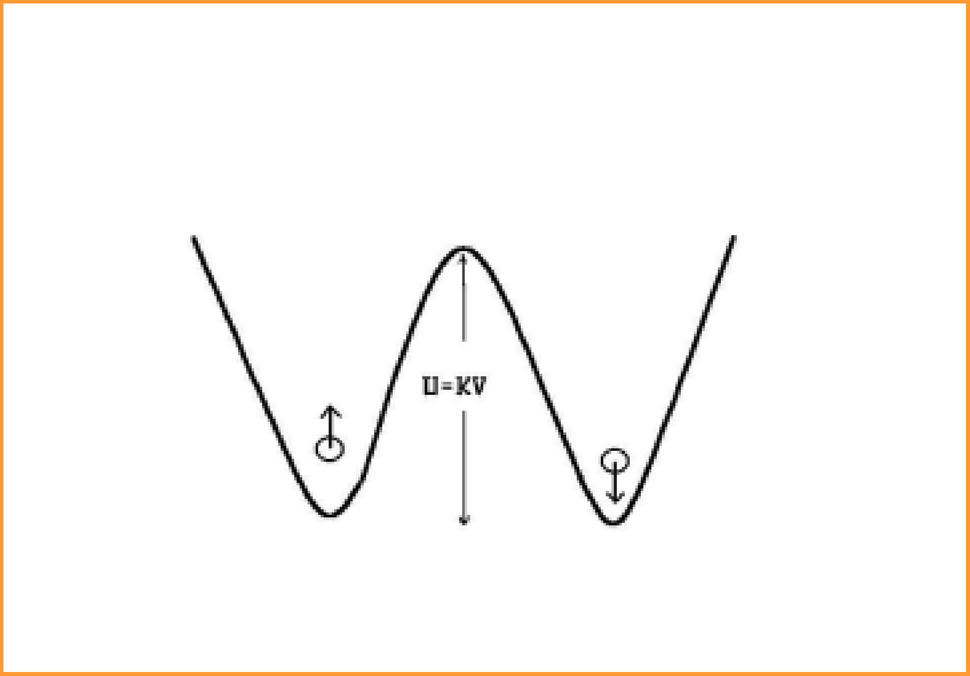

.As the size of nanoparticles decreases,when KV< k_BT, magnetic nanoparticles exhibit superparamagnetic relaxation, i.e., thermally fluctuations of the magnetization vector among the easy axis of magnetization.

Macroscopic quantum coherence?

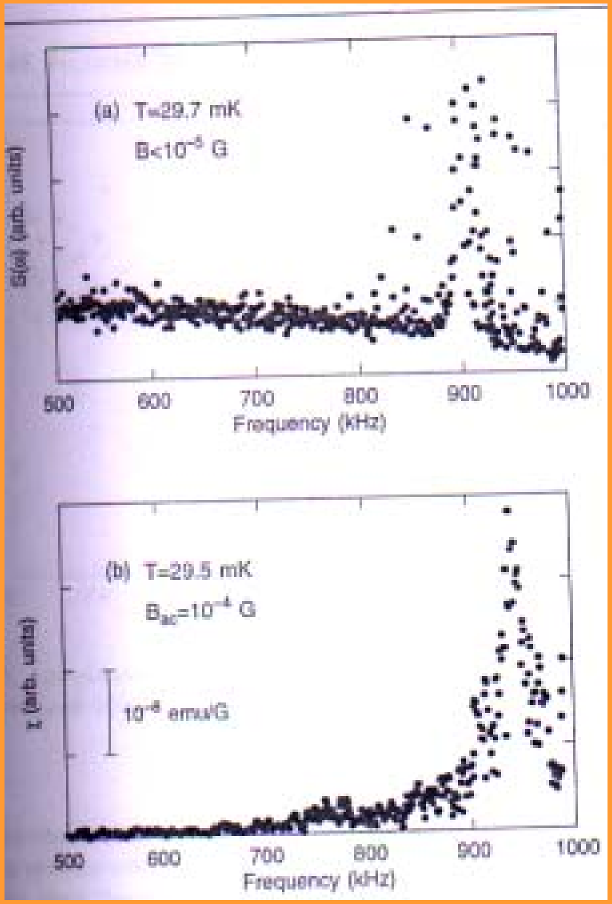

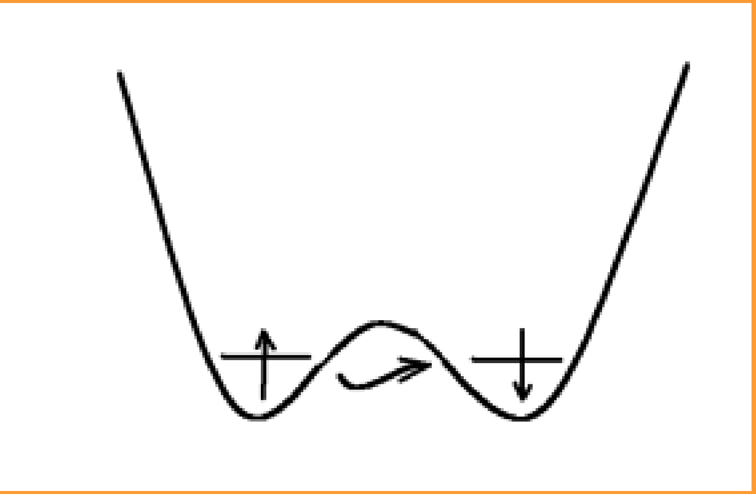

SPR of Fe_3O_4 Size II

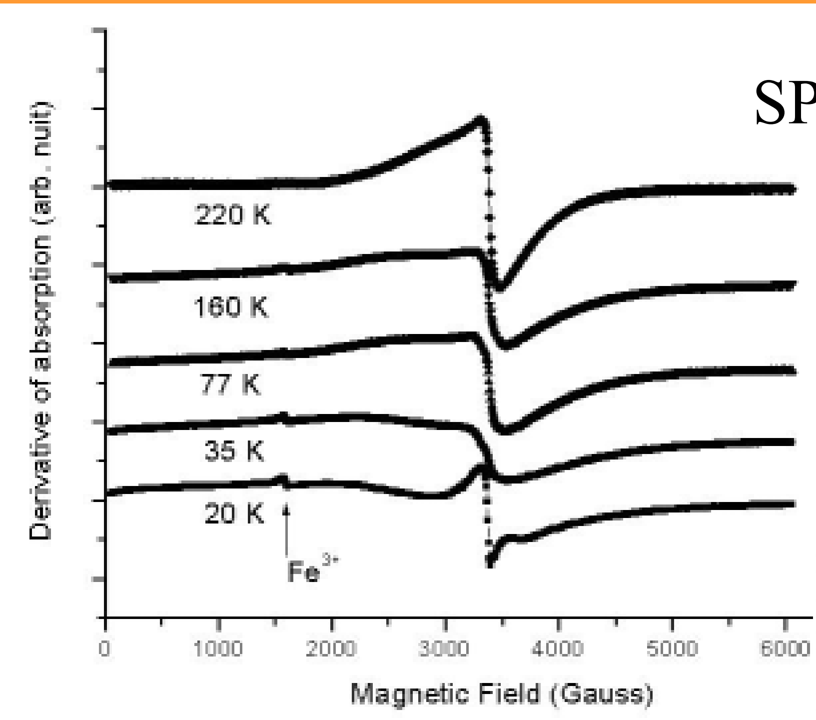

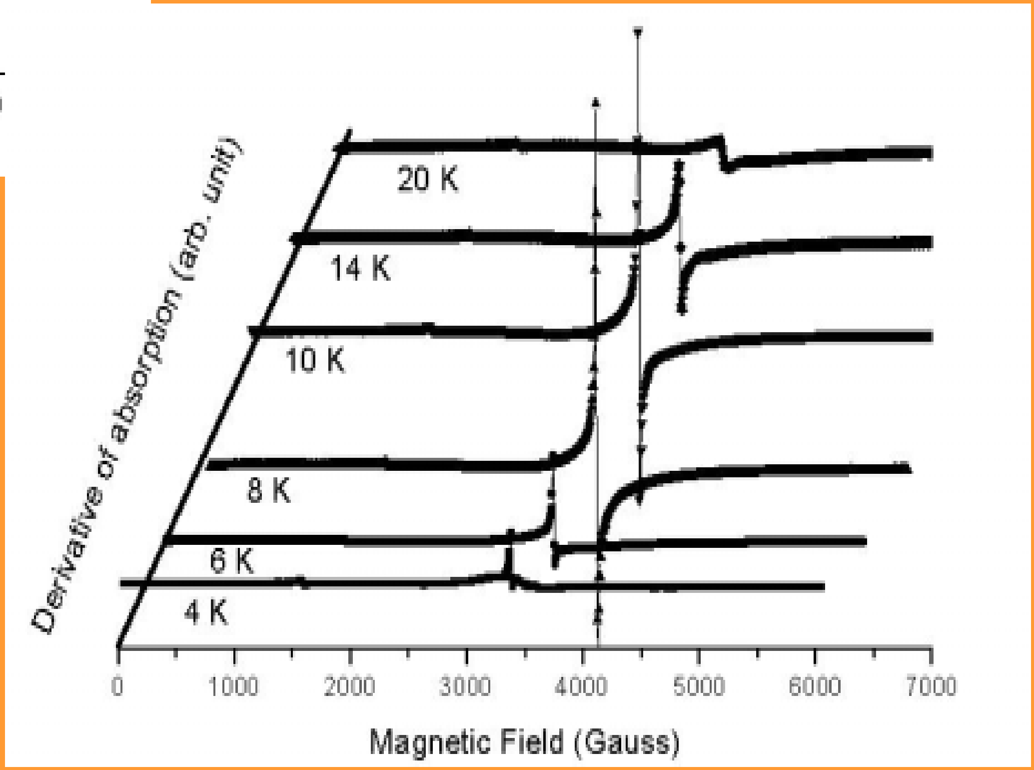

Speculative diagram for surface
…uced quantum
…ansition

Physical pictures of magnetic nanoparticles

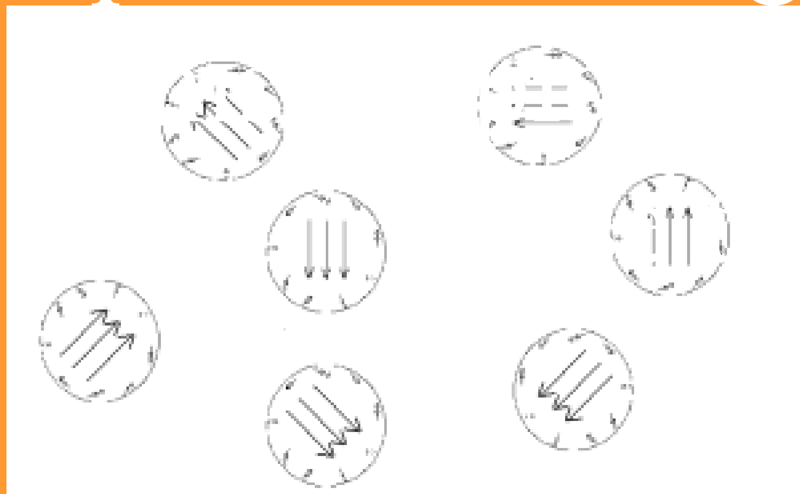

Superparamagnetism

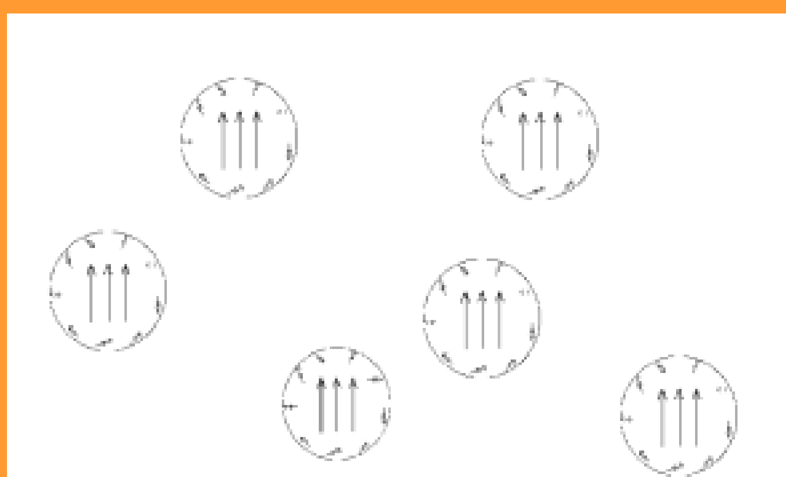

Ferromagnetism

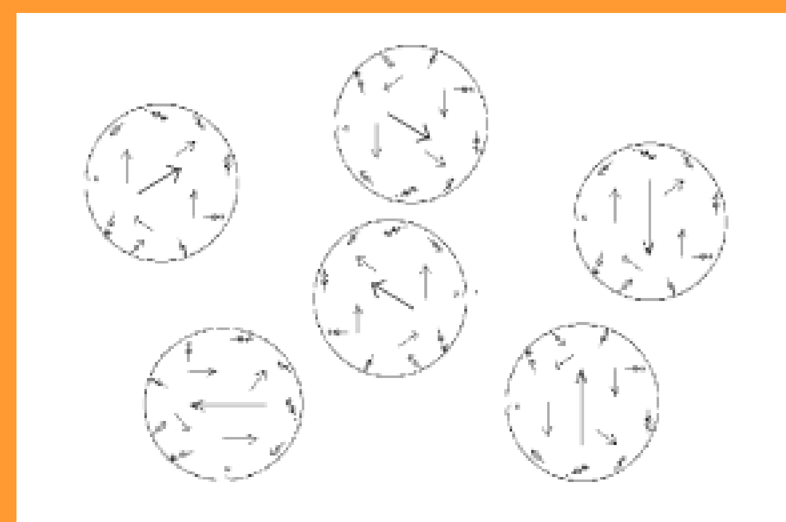

Quantum paramagnetism

Geomagnetic intensity & magnetic declination

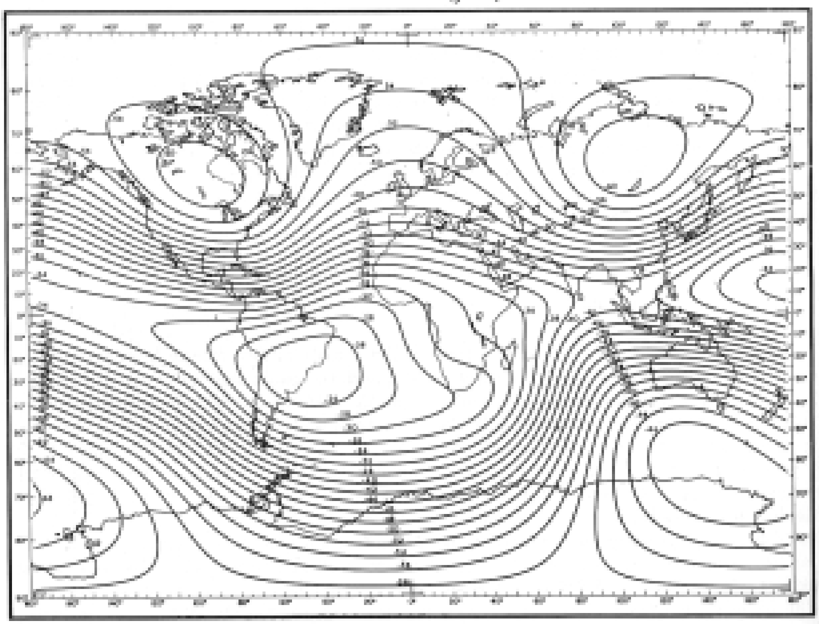

Figure 3. Total geomagnetic intensity, IGRF 1965.0. From Zmuda (1971) with permission.

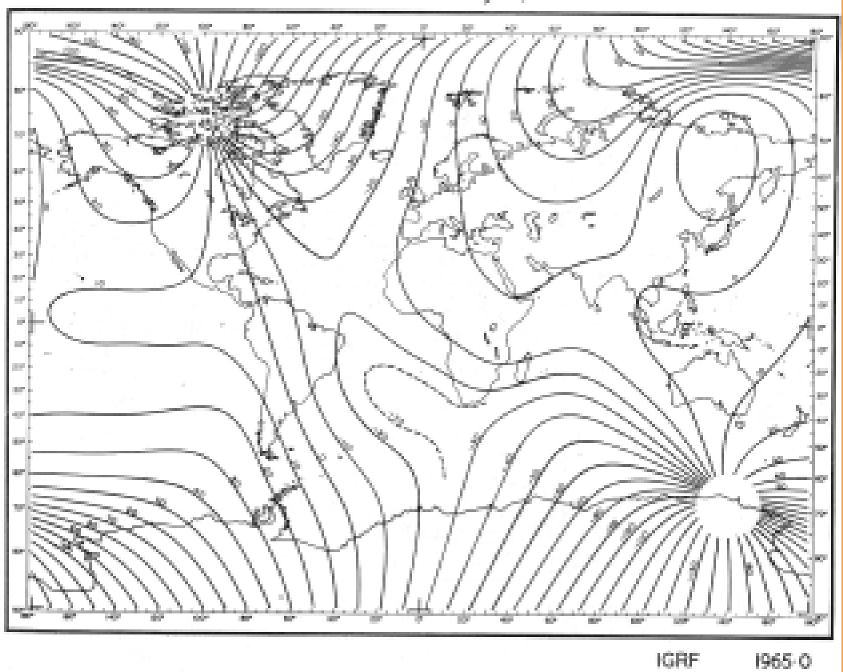

Figure 4. Magnetic declination, IGRF 1965.0. From Zmuda (1971) with permission.

Iron-containing cells (trophocytes) and fat cells (oenocytes)

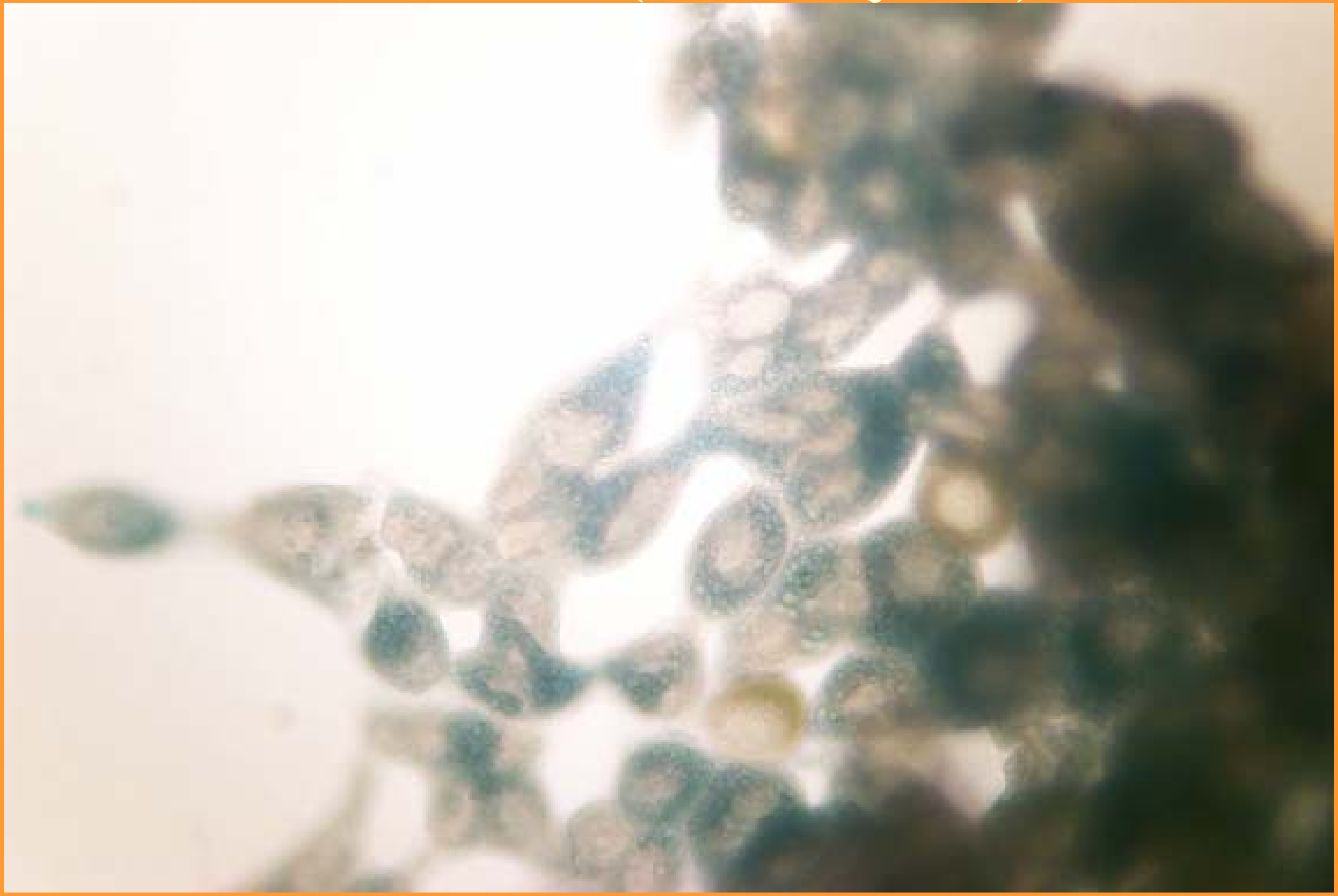

純化樣品A之EPR變溫光譜圖(30k-4k)

(b)MFM實驗數據

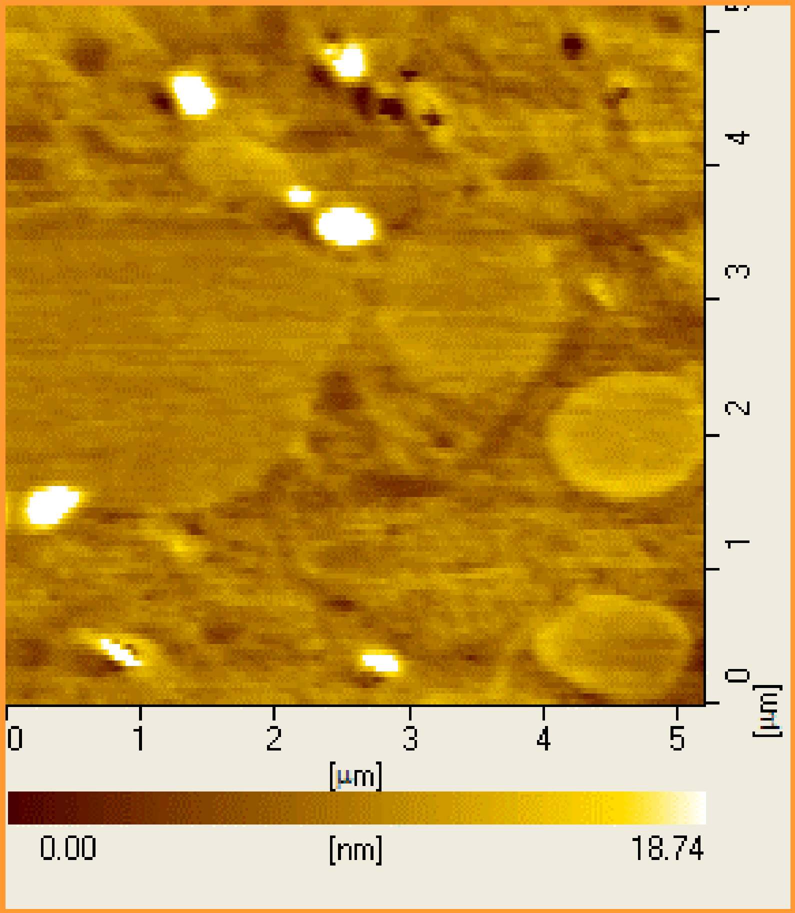

AFM之表面影像

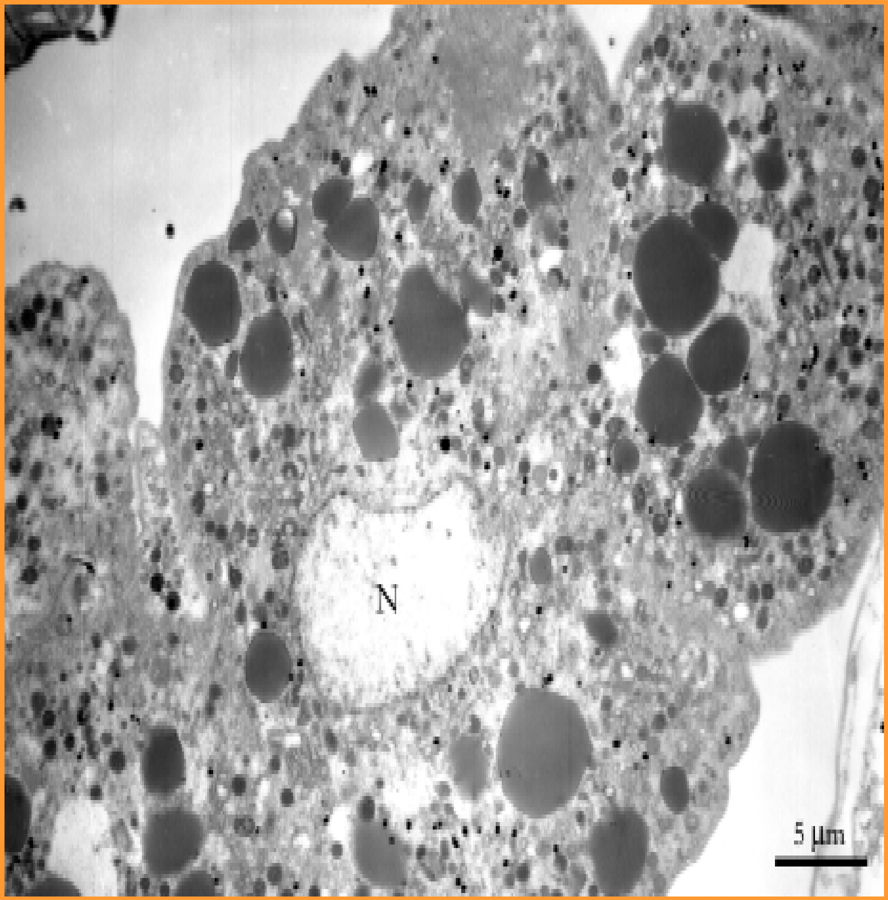

TEM影像

改變外加磁場方向，所獲的MFM之影像(鱒魚)

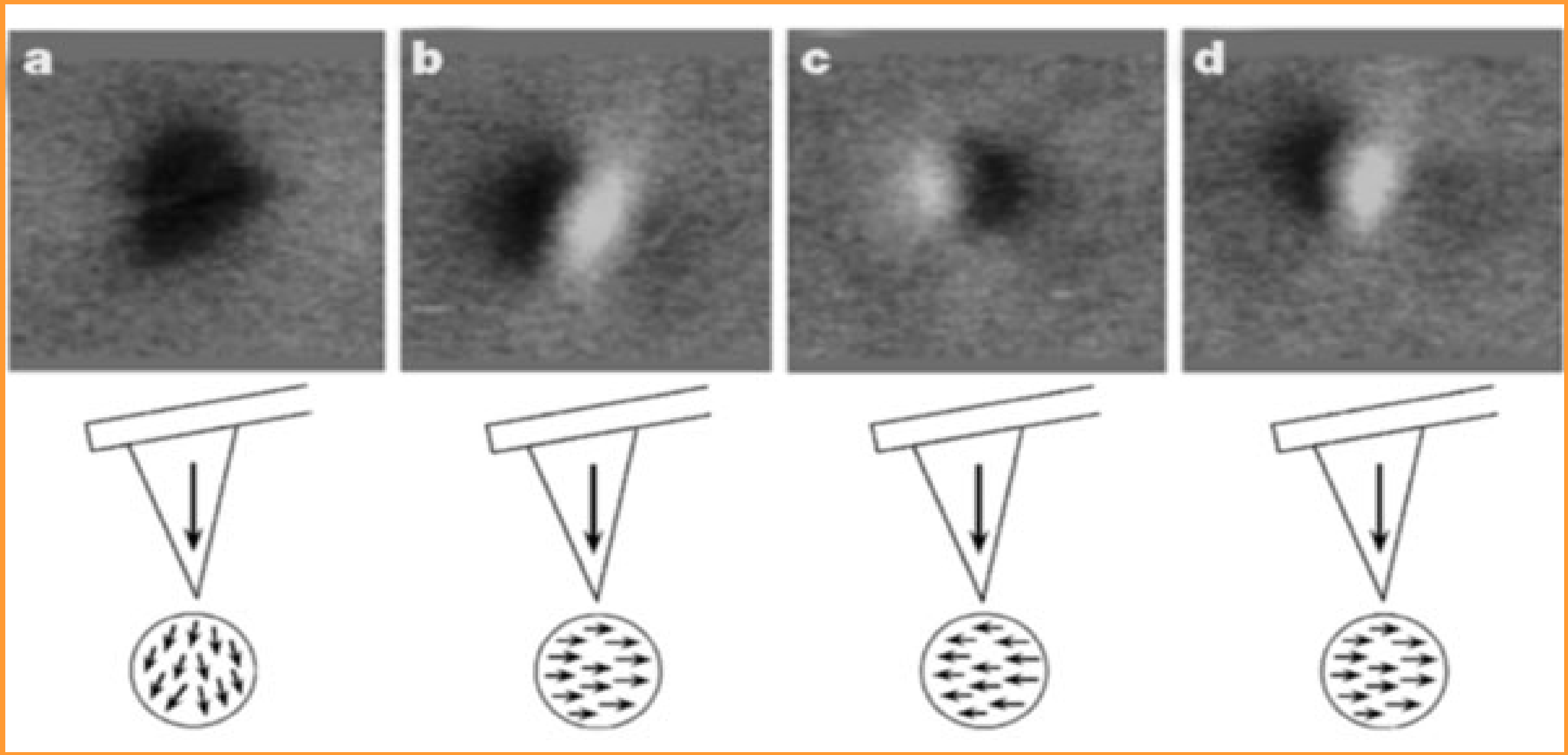

Diebel, C. E. et al. *Nature* **406**, 299 (2000)

MFM之表面影像與phase影像

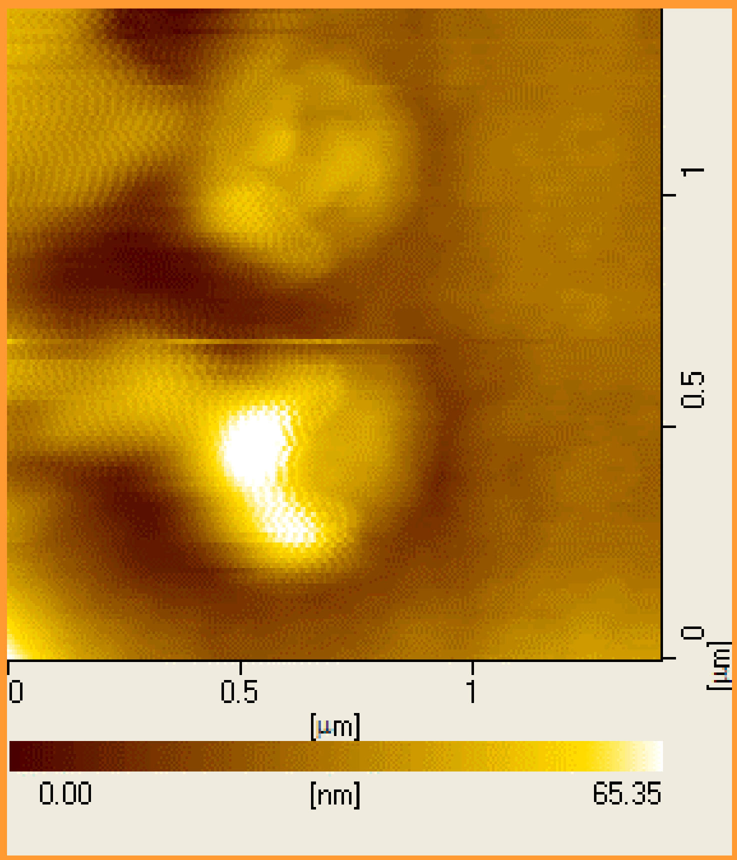

MFM之表面影像

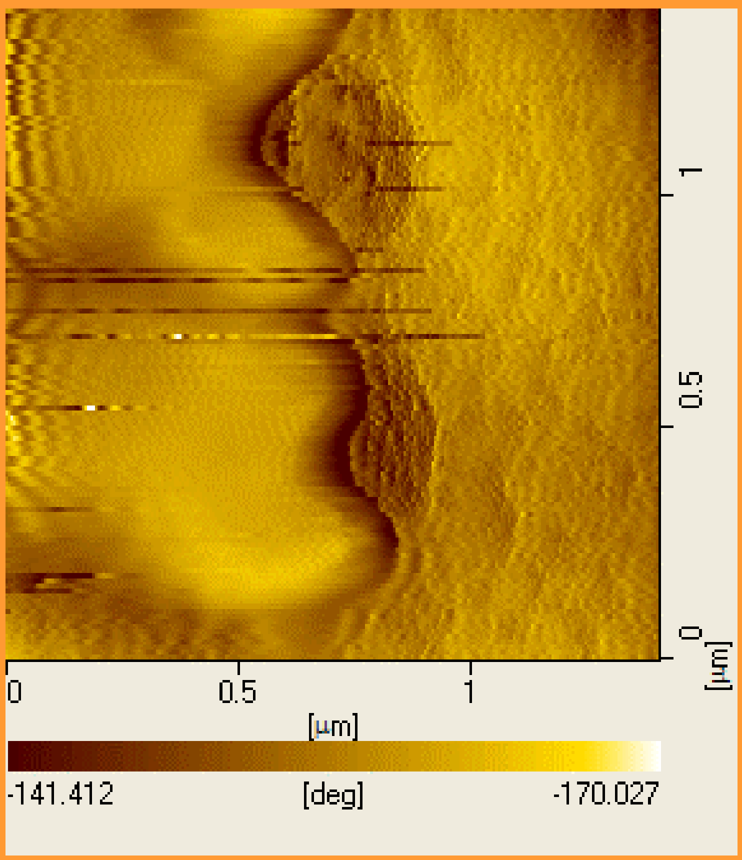

MFM之phase影像